ФИЗИКА ЭЛЕМЕНТАРНЫХ ЧАСТИЦ И АТОМНОГО ЯДРА
2007. Т. 38. ВЫП. 3

REVIEW OF THE TOP-QUARK MASS MEASUREMENT AT THE CDF IN $p\bar{p}$ COLLISIONS AT $\sqrt{s} = 1.96$ TeV

J. A. Budagov, V. V. Glagolev, I. A. Suslov

Joint Institute for Nuclear Research, Dubna

Upgraded Tevatron Run-II luminosity has opened a new chapter in modern heavy-quark studies — *a top physics*: a dozen level of a Tevatron Run-I top-events statistics now is being replaced by hundreds of events. A review is made of a mass measurement of the top quark produced at $\sqrt{s} = 1.96$ TeV in $p\bar{p}$ collisions at the Collider Detector at Fermilab (CDF) with the integrated luminosity samples up to 359 pb^{-1}. Review covers the M(top) measurement using mainly the so-called template methods both in «lepton + jets» and «dilepton» channels of top-quark decay. The CDF top-quark mass obtained in lepton + jets mode is currently the world most precise single measurement of this important physics parameter. Work summarizes the essential results of the CDF top-quark mass measurement achieved and published for the recent 2003–2005 period.

Статистика протон-антипротонных взаимодействий, накопленная на модернизированном тэватроне во втором сеансе, открывает новый раздел в современном изучении тяжелых кварков — физику топ-кварков: десятки событий с распадами топ-кварков в первом сеансе тэватрона заменяются сотнями. В обзоре рассматриваются измерения массы топ-кварков, рожденных в протон-антипротонных взаимодействиях при энергии $\sqrt{s} = 1{,}96$ ТэВ на установке CDF (Fermilab) при накопленной светимости до 359 пб$^{-1}$. Обзор посвящен, в основном, измерениям массы топ-кварка с помощью так называемых «шаблонных методов» для двух каналов распада топ-кварка: однолептонного и двухлептонного. Измерение массы топ-кварка на CDF в однолептонном канале является на данный момент наиболее точным отдельным измерением этого важного физического параметра. Работа суммирует наиболее весомые результаты измерения массы топ-кварка на установке CDF, полученные и опубликованные в период 2003–2005 гг.

PACS: 14.65.Ha

INTRODUCTION

The top quark, the weak isospin partner of the bottom quark (Table 1), was first observed by the CDF and DØ collaborations in $p\bar{p}$ collisions produced at the Fermilab Tevatron [1].

During Run-I operation from 1992 to 1995, CDF acquired 110 pb^{-1} of data at a center-of-mass energy of 1.8 TeV, and performed the first measurements of top-quark properties. Since the Run-II start at the Tevatron in 2001, CDF has collected integrated luminosities several times that of Run-I. Increased top production from a higher collision energy and improved acceptance of the upgraded detector have

further enhanced the Run-II top-quark yield. This larger sample size allows for more precise studies of the characteristics of the top-quark.

Table 1. **The quark quantum numbers**

Generation	Symbol	Q/e	Weak isospin	Flavour
1	u	$+2/3$	$1/2$	$I_z = 1/2$
1	d	$-1/3$	$-1/2$	$I_z = 1/2$
2	s	$-1/3$	$-1/2$	$S = -1$
2	c	$+2/3$	$1/2$	$C = 1$
3	b	$-1/3$	$-1/2$	$B' = -1$
3	t	$+2/3$	$1/2$	$T = 1$

As with all quarks, the top-quark mass is not predicted by theory, and therefore represents a free parameter in the standard model which must be experimentally determined. Tevatron Run-I measurements yielded the top-quark mass of (178.0 ± 4.3) GeV/c^2 [2], approximately 40 times heavier than the bottom quark. Such a large mass, close to the electroweak symmetry breaking scale $v = (\sqrt{2}G_F)^{-1/2} \simeq 246$ GeV, suggests that the top quark may have a special role in electroweak symmetry breaking scale process [3]. The large contribution to quark-loop corrections of electroweak parameters from the heavy top quark provides for powerful tests of the standard model. In particular, a precise measurement of the top-quark mass, coupled with that of the W boson, leads to tighter constraints on the as yet unobserved Higgs boson [4].

At the Tevatron, in the Run-II $p\bar{p}$ collisions with a center-of-mass energy of 1.96 TeV, top quarks are produced mainly in $t\bar{t}$ pairs, through $q\bar{q}$ annihilation ($\sim 85\%$) and gluon–gluon fusion. Because of its large decay width and correspondingly short lifetime ($\sim 4 \cdot 10^{-25}$ s), the top quark decays before any hadronization can take place, so that its existence as a «free quark» can be studied without the complication of lower energy QCD effects. In the framework of the standard model, each top quark decays almost exclusively to a W boson and a bottom quark. The b quark hadronizes into a jet of particles, while the W decays either to a $q\bar{q}'$ or a lepton–neutrino pair. Thus, the decays of the W bosons determine the characteristics of a $t\bar{t}$ event and, consequently, the event selection strategy.

The «all hadronic» mode, where both Ws decay into $q\bar{q}'$ pairs, occurs for $\sim 44\%$ of $t\bar{t}$ events, but this topology is dominated by a large QCD multijet background. The most precise top-quark mass measurements arise from the «lepton + jets» mode ($\sim 30\%$ of events), where one W decays hadronically: $t\bar{t} \to b\ell\nu_\ell\bar{b}q\bar{q}'$, while the other decays to either an electron or muon plus a neutrino, whose presence can be inferred from missing transverse energy in the detector. A third mode occurs when both W bosons from each top quark decay into leptons: $t\bar{t} \to \bar{b}\ell^-\overline{\nu}_\ell b\ell'^+\nu'_\ell$. Though this «dilepton» mode accounts for only $\sim 5\%$ of $t\bar{t}$

events (without counting tau-lepton decays), such measurements are important as they allow one to reduce the overall uncertainty on the top-quark mass. Further, dilepton measurements test the consistency of top-quark mass results obtained using other decay modes, as the dilepton mode contains different background sources and, therefore, represents an inherently different event sample. Since all top-quark mass measurements assume a sample composition of $t\bar{t}$ and standard model background events, any discrepancy among the measured top masses could indicate the presence of new physics processes.

Till now CDF II reconstructs the top-quark mass only in two «purest» decay modes: «lepton + jets» and «dilepton». There are several top-quark mass reconstruction methods developed for each of mentioned decay mode. The methods could be subdivided into two main classes: 1) template methods and 2) Matrix Element Technique methods. Dubna group measured the top-quark mass using the template methods both in l + jets and dilepton channels of top-quark decay [5–7]. The top-quark mass obtained in l + jets mode [8], with Dubna group participation, is the most precise current single measurement on this important physical parameter.

Review will focus mainly on the template methods and give only a short description of the Dynamical Likelihood Method (DLM) [9] as a representative of the Matrix Element Technique methods.

1. DETECTOR AND EVENT SELECTION

The data sample used for these analyses was collected by the Collider Detector at Fermilab [10] during Run-II operation between March 2002 and August 2004. As depicted in Fig. 1, the CDF II is an azimuthally and forward–backward symmetric apparatus designed to study $p\bar{p}$ reactions at the Tevatron. We use a cylindrical coordinate system about the proton beam axis in which θ is the polar angle, ϕ is the azimuthal angle, and pseudorapidity is defined as $\eta \equiv -\ln[\tan(\theta/2)]$. The detector has a charged-particle tracking system immersed in a 1.4 T magnetic field, aligned coaxially with the $p\bar{p}$ beams. The Run-II Silicon Vertex Detector (SVX II) and Intermediate Silicon Layer (ISL) provide tracking over the radial range from 1.5 to 28 cm [11]. A 3.1 m long open-cell drift chamber, the Central Outer Tracker (COT), covers the radial range from 40 to 137 cm [12]. The fiducial region of the silicon detector extends to pseudorapidity $|\eta| \sim 2$, while the COT provides coverage for $|\eta| \lesssim 1$.

Segmented electromagnetic and hadronic sampling calorimeters surround the tracking system and measure the energy flow of interacting particles in the pseudorapidity range $|\eta| < 3.6$. Dilepton analysis uses the new end-plug detectors [13] to identify electron candidates with $1.2 < |\eta| < 2.0$ in addition to the central detectors [14] for lepton candidates with $|\eta| < 1.1$. A set of drift chambers and

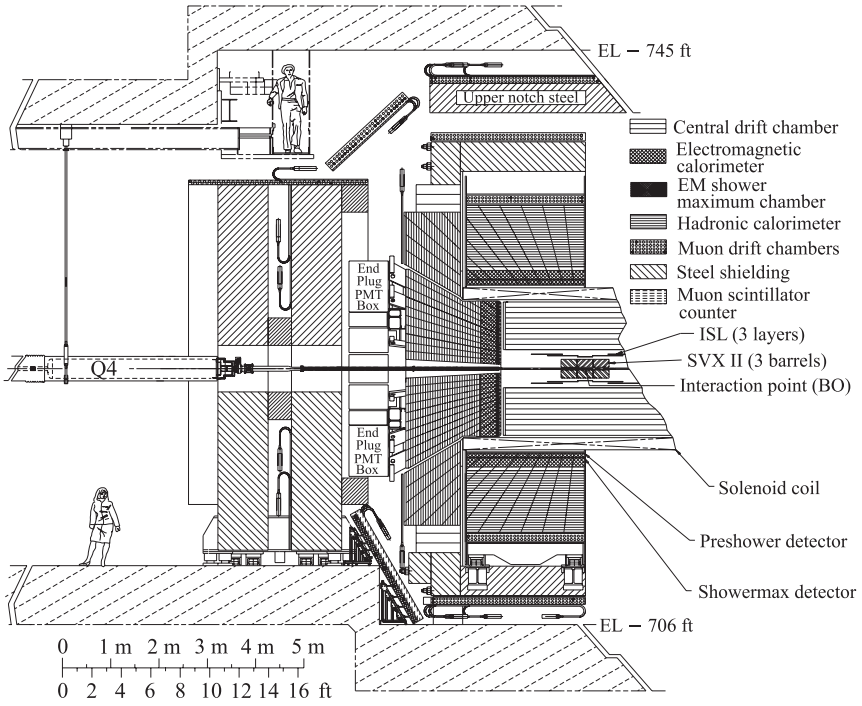

Fig. 1. Elevation view of the CDF II detector, showing the inner silicon microstrip detector, central outer tracker drift chamber, electromagnetic and hadronic calorimeters, and muon drift chambers and scintillation counters

scintillation counters [15] are located outside the central hadron calorimeters; and another set, behind a 60 cm iron shield to detect muon candidates with $|\eta| \lesssim 0.6$. Additional chambers and counters detect muons in the region $0.6 \leqslant |\eta| \leqslant 1.0$. Gas Cherenkov counters [16] located in the $3.7 < |\eta| < 4.7$ region measure the average number of inelastic $p\bar{p}$ collisions per bunch crossing and thereby determine the beam luminosity.

1.1. Lepton + Jets Selection. A data sample enriched in $t\bar{t}$ events in the lepton + jets channel is selected by looking for events with an electron (muon) with $E_T > 20$ GeV ($p_T > 20$ GeV/c), missing transverse energy $\not\!\!E_T > 20$ GeV, at least three jets with $E_T > 15$ GeV, and the fourth jet with $E_T > 8$ GeV.

Selected events must contain exactly one well-identified lepton candidate in events recorded by the high-p_T lepton triggers. The lepton candidate can be a central electron or a muon. The trigger efficiencies for leptons in the final sample are high, $\sim 96\%$ for electrons and $\sim 90\%$ for muons, and show negligible p_T dependence.

Jets can be identified as b jets using a displaced vertex tagging algorithm, which proceeds as follows. The primary event vertex is identified using a fit to all prompt tracks in the event and a beamline constraint. The beamline is defined as a linear fit to the collection of primary vertices for particular running periods. The luminous region described by the beamline has a width of approximately 30 μm in the transverse view and 29 cm in the z direction. Jets with $E_T > 15$ GeV are checked for good-quality tracks with both COT and silicon information. When a secondary vertex can be reconstructed from at least two of those tracks, the distance between the primary and secondary vertices along the jet direction in the plane transverse to the beams L_{2D} is calculated, along with its uncertainty $\sigma(L_{2D})$. If $L_{2D}/\sigma(L_{2D}) > 7.5$, the jet is considered tagged. The per-jet efficiency for b jets in the central region is shown as a function of jet E_T in Fig. 2; the algorithm has an efficiency of about 60% for tagging at least one b jet in a $t\bar{t}$ event. More information concerning b tagging is available elsewhere [17].

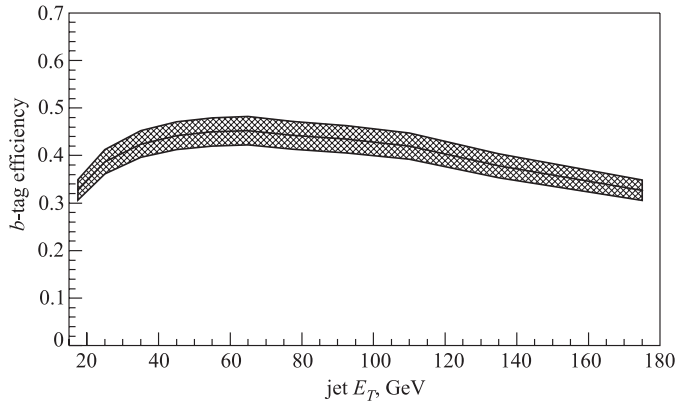

Fig. 2. The efficiency of the secondary vertex b-tagging algorithm is shown as a function of jet E_T for b jets in the central region of the detector ($|\eta| < 1$), where the tracking efficiency is high. The shaded band gives the $\pm 1\sigma$ range for b-tagging efficiency

The signal-to-background ratio was improved by requiring in each event the presence of four or more jets with $|\eta| < 2.0$. To reduce backgrounds further one required either (a) at least four jets with transverse energy $E_T > 21$ GeV or (b) at least three jets with $E_T > 15$ GeV and the fourth jet with $E_T > 8$ GeV with at least one jet with $E_T > 15$ GeV identified as a b quark candidate through the presence of a displaced vertex within the jet arising from the decay of the long-lived bottom hadron (b tag). This selection resulted in 165 events that, based on background estimates, are primarily $t\bar{t}$ events. The methods used to estimate the backgrounds are detailed in [17].

The «dynamical likelihood method» (DLM) analysis [9] uses a 63-event subset of those data defined by requiring exactly four jets with $E_T > 15$ GeV where at least one of the jets has a b tag. The various sources of background contamination in this sample are summarized in Table 2 to be (9.2 ± 1.8) events.

Table 2. **The background composition and the number of $t\bar{t}$ candidates for events with $\geqslant 1$ b tag, and for the subset used in the DLM analysis**

Sample	$\geqslant 1$ b tag	DLM sample
Source	Expected Background	
$W +$ jets	19.6 ± 2.4	5.3 ± 1.1
Multijet	4.7 ± 0.7	3.1 ± 1.0
Other	2.3 ± 0.2	0.8 ± 0.1
Total	26.6 ± 3.0	9.2 ± 1.8
	Selected $t\bar{t}$ Candidates	
Data	121	63

The template method [8] divides 165 events into four nonoverlapping subsamples with different background levels. Ordered by decreasing statistical power, the subsamples are 1) events with at least four jets with $E_T > 15$ GeV and one b-tagged jet («1-tag Tight» sample with 63 events), 2) events with two or more b-tagged jets («2-tag» sample with 25 events), 3) events with the fourth jet with $8 < E_T < 15$ GeV and one b-tagged jet with $E_T > 15$ GeV («1-tag Loose» sample with 33 events), and 4) events with four jets with $E_T > 21$ GeV and no b-tagged jets («0-tag» sample with 44 events). The estimated background levels in the samples with a b tag are summarized in Table 2. The background level in the 0-tag sample is determined in the subsequent fit.

1.2. Dilepton Selection. The signature of $t\bar{t}$ decays in the dilepton channel is two jets from the b quarks, two high-momentum leptons and large missing energy (due to the unobserved neutrinos) from the W decays, and the possibility of extra jets from initial or final-state radiation. The major backgrounds for dilepton $t\bar{t}$ events are from Drell–Yan dilepton production ($q\bar{q} \to Z/\gamma^* \to e^+e^-, \mu^+\mu^-, \tau^+\tau^-$), $W(\to \ell\nu) +$ jets events where a jet «fakes» the signature of a lepton, and diboson production (WW, WZ, ZZ) [18].

The data are derived from inclusive lepton triggers demanding central electrons ($|\eta| < 1.1$) with transverse energy $E_T > 18$ GeV, or central muons ($|\eta| < 1.1$) with transverse momentum $p_T > 18$ GeV/c . Electrons in the end plug are required to have $E_T > 20$ GeV. Events must also have a missing transverse energy $\not\!\!E_T > 25$ GeV, calculated from the vector sum of $-\sum_i E_T^i \mathbf{n}_i$, where $\mathbf{n}_i$ is the unit vector in the azimuthal plane which points from the beam line to the ith calorimeter tower.

The top-quark mass dilepton analyses described here employ one of two sets of selection criteria developed for the $t\bar{t}$ cross section measurement in the dilepton decay channel [18]. The first method, referred to as the «dilepton»

(DIL) analysis, is similar to that used in the CDF Run-I measurement [19], and requires both candidate leptons to be specifically identified as either electrons or muons. The second «lepton+track» (LTRK) method increases the efficiency of the event selection (at the cost of a larger background) by requiring one well-identified lepton (electron or muon) in conjunction with an isolated track with large transverse momentum. This method recovers events where leptons fall in calorimeter or muon detector gaps, and increases the acceptance for single prong hadronic decays of the τ lepton from $W \to \tau\nu$ (approximately 20% of the total LTRK acceptance, compared with 12% for the DIL selection).

Both selection methods demand a «tight» lepton in combination with a «loose» lepton of an opposite charge. Requirements for the tight lepton are identical for both methods, but differ for the loose lepton. Tight leptons must have well-measured tracks, based on the numbers of silicon and drift chamber hits and reconstructed vertex position, and have $E_T > 20$ GeV. Tight leptons must also satisfy the isolation requirement that the total calorimeter E_T within a cone $\Delta R \equiv \sqrt{\Delta\eta^2 + \Delta\phi^2} = 0.4$ about the lepton trajectory not exceeds 10% of the lepton's E_T. Tight electrons must have lateral and longitudinal electromagnetic shower profiles in the calorimeter consistent with electrons, while tight muons must point to muon chamber hits and have a calorimeter signature compatible with minimum-ionizing particles. For the DIL method, loose leptons must be well-identified electrons or muons with no isolation requirement. Loose DIL electrons must be central, while the muon chamber hit requirements for loose DIL muons are relaxed. Loose leptons in the LTRK method, in contrast, are simply required to be well-measured and isolated tracks within $|\eta| < 1$ and having $p_T > 20$ GeV/c. The LTRK loose lepton isolation is determined from the p_T sum of neighboring tracks within the cone $\Delta R = 0.4$ about the lepton track, which must not exceed 10% that of the lepton.

At least two jets are required per event, and are derived from looking for clusters of energy in calorimeter towers within a cone size of $\Delta R = 0.4$. This total jet E_T is corrected for nonuniformities in the response of the calorimeter as a function of η, effects from multiple $p\bar{p}$ collisions, and the hadronic jet energy scale of the calorimeter [20]. Jets are required to have $|\eta| < 2.5$ and $E_T > 15$ GeV for the DIL analysis, or $|\eta| < 2.0$ and $E_T > 20$ GeV for the LTRK method. The two highest E_T jets for each event are assumed to stem from the b quarks; this assumption is true for $\sim 70\%$ of simulated $t\bar{t}$ events. The momentum components of each b quark are then calculated from the measured jet E_T and angle by assuming a b-quark mass of 5.0 GeV/c^2. No identification of b jets is used.

The final signature of a dilepton $t\bar{t}$ event is missing transverse energy $\not\!\!E_T$ in the calorimeter. Dilepton $t\bar{t}$ events should satisfy the requirement $\not\!\!E_T > 25$ GeV. False $\not\!\!E_T$ may arise through mismeasurement of the leptons or jets. Therefore,

both DIL and LTRK methods require a minimum angular separation $\Delta\phi$ between lepton or jet trajectories and the $\not\!\!E_T$ vector. For the DIL selection, events must have $\Delta\phi > 20^\circ$ for all leptons and jets if $\not\!\!E_T < 50$ GeV. In the LTRK method, the $\not\!\!E_T$ vector cannot be within 5° of either the tight lepton direction or the axis of the loose lepton, and jets must have $\Delta\phi > 25^\circ$ for events with $\not\!\!E_T < 50$ GeV.

The dominant source of background for both selection methods is from Drell–Yan ($q\bar{q} \to Z/\gamma^* \to ee, \mu\mu$) events. These events should have no real $\not\!\!E_T$, and can only satisfy the selection criteria if there is mismeasurement of the lepton or jet E_T. Therefore, additional selection requirements are imposed for events where the reconstructed invariant mass of the two lepton candidates lies within 15 GeV/c^2 of the Z boson resonance. For these events, the DIL method requires a «jet significance» of > 8, defined as the ratio of $\not\!\!E_T$ to the sum of jet E_T projected along the $\not\!\!E_T$ direction. The LTRK method increases the $\not\!\!E_T$ requirement to $\not\!\!E_T > 40$ GeV for dilepton events near the Z resonance. The DIL method further suppresses background processes by requiring that the scalar sum of jet E_T, lepton p_T, and $\not\!\!E_T$ (denoted by H_T) exceeds 200 GeV.

Table 3. **Luminosity, expected $t\bar{t}$ signal and background (with total uncertainties), and observed number of events for the DIL and LTRK selection methods. A $t\bar{t}$ cross section of 6.1 pb is assumed, corresponding to a top mass of 178 GeV/c^2**

Selection method	DIL	LTRK
Luminosity, pb^{-1}	340	360
Expected $t\bar{t}$	15.7 ± 1.3	19.4 ± 1.4
Drell–Yan	5.5 ± 1.2	8.7 ± 3.3
$W(\to \ell\nu)$ + jets fakes	3.5 ± 1.4	4.0 ± 1.2
Diboson	1.6 ± 0.3	2.0 ± 0.4
Total background	10.5 ± 1.9	14.7 ± 3.6
Total expected	26.2 ± 2.3	34.1 ± 3.9
Observed	33	46

Table 3 summarizes the luminosity and expected numbers of signal and background events for the DIL and LTRK selection methods, along with observed results from the inclusive lepton data set. The LTRK selection comprises a 6% greater luminosity since it is able to accept $e\mu$ dilepton decays when muon detectors were not operational. The acceptance and efficiency of $t\bar{t}$ signal events are calculated with a full detector simulation using PYTHIA [21] Monte Carlo and assuming a production cross section of 6.1 pb, corresponding to a top mass of 178 GeV/c^2 [22]. The Drell–Yan, $W(\to \ell\nu)$ + jets fakes, and diboson background acceptances are estimated using a combination of Drell–Yan and W + jets data, and PYTHIA and ALPGEN + HERWIG [23, 24] simulations. The total

uncertainties for expected event yields include both the statistical uncertainties of the Monte Carlo samples used, as well as systematic uncertainties from particle identification, jet energy measurement, and modelling of the $t\bar{t}$ signal and background. Applied to the inclusive lepton data set, the DIL selection observes 33 events, and the LTRK selection observes 46 events. The DIL and LTRK data samples share 24 events in common, leading to a union of 55 events with a 44% overlap [28].

2. METHODS FOR TOP-MASS MEASUREMENT

There are several CDF II methods developed for top-mass measurement which can be subdivided into two groups: «Template methods» and «Matrix Element Technique methods». We review mainly «Template methods» and give a short description of a «dynamical likelihood method» (DLM) as a representative of the «Matrix Element Technique methods».

2.1. Lepton + Jets Methods. *2.1.1. «Dynamical Likelihood Method» (DLM).* The DLM technique, described in detail in [9], defines a likelihood for each event based on the differential cross section per unit phase space volume of the final-state partons, $d\sigma_{t\bar{t}}/d\Phi$, as a function of $M_{\rm top}$. Detector resolution effects are accounted for using $t\bar{t}$ events generated by the HERWIG Monte Carlo program [24] and full detector simulation to derive a transfer function (TF). The TF relates the transverse energies of the quarks, denoted by $\mathbf{x}$, and the observed jets. For a given event, a Monte Carlo integration is performed over the possible $t\bar{t}$ final state kinematics in the following way: generate a random value for the virtual mass squared of the W boson in the leptonic channel, s_W, according to the Breit–Wigner form. The momentum of the electron or muon daughter is identified with the measured value, and the neutrino transverse momentum with the measured missing transverse energy. Then random values for the momenta of final state quarks according to the TF probabilities are generated. The z component of the neutrino momentum, with a two-fold ambiguity, is determined using s_W as a constraint. Thus, for a given set of $\mathbf{x}$ and s_W, one fully determines the event kinematics, and the event likelihood as a function of $M_{\rm top}$ is given by

$$L(M_{\rm top}) = N \sum_{I_j} \sum_{I_\nu} \frac{d\sigma_{t\bar{t}}}{d\Phi}(M_{\rm top}; \mathbf{x}, s_W), \tag{1}$$

where the normalization factor N is independent of $M_{\rm top}$ for a given event, and the indices I_j and I_ν run over the parton-jet assignments and the two neutrino solutions, respectively. The event likelihood is obtained by numerically integrating over $\mathbf{x}$ given by the TF and s_W given by the Breit–Wigner distribution.

Figure 3 shows the distribution of the top-quark mass value at the point of maximum likelihood in each event compared with the expectation from simulated

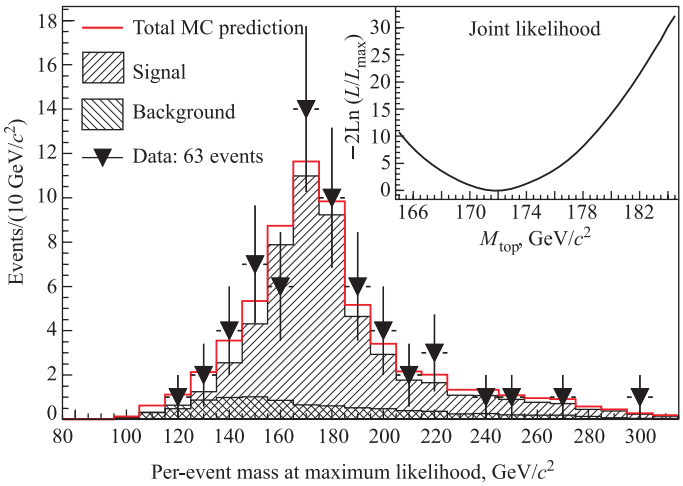

Fig. 3. The value of the top-quark mass at the maximum of the DLM likelihood is plotted for each event. Data events (points) are compared to an expected distribution (histogram) comprising simulated $t\bar{t}$ ($M_{\mathrm{top}} = 172.5$ GeV/c^2) and background events. The last bin includes events with masses > 305 GeV/c^2. The inset shows the joint log-likelihood for the 63 events, before accounting for the presence of background

events. An inset shows the joint log-likelihood as a function of M_{top}, formed by multiplying the likelihoods of the individual events together.

2.1.2. Template Method. In this section, we describe the procedures [8] for determining in each event the reconstructed top-quark mass m_t^{reco} and the dijet mass m_{jj}, representing the mass of the hadronically decaying W boson. Remember that m_t^{reco} is not an event-by-event measurement of the top-quark mass; rather it is a quantity whose distribution in the data will be compared with simulated samples to extract the top-quark mass. Similarly, the distribution of m_{jj} will be used to constrain the calibration of the jet energy scale (JES) in the reconstructed events.

Throughout the mass reconstruction, each event is assumed to be a $t\bar{t}$ event decaying in the lepton + jets channel, and the four leading jets are assumed to correspond to the four quarks from the top and W decays. First, the measured four-vectors for the jets and lepton in the event are corrected for known effects, and resolutions are assigned. Next, for the top-quark mass reconstruction, a χ^2 fit is used to extract the reconstructed mass, so that each event has a particular value of m_t^{reco} and a corresponding χ^2 value. Some events are discarded from the event sample when their minimized χ^2 exceeds a cut value. Meanwhile, for

the dijet mass reconstruction, the invariant mass m_{jj} is calculated for each pair of jets without b tags among the leading four jets.

All of the transverse energy in the calorimeter (towers with $|\eta| < 3.6$) that is not associated with the primary lepton or one of the leading four jets is considered «unclustered energy». Each transverse component of the unclustered energy (p_x^{UE}, p_y^{UE}) is assigned an uncertainty of $0.4\sqrt{\sum E_T^{\mathrm{uncl}}}$, where $\sum E_T^{\mathrm{uncl}}$ is the scalar sum of the transverse energy excluding the primary lepton and leading four jets. The uncertainty comes from studies of events with no real missing energy and no hard jet activity.

The unclustered energy is the observed quantity and the input to the χ^2 fit, but it is related to the missing energy through the other measured physics objects in the event, since the $p\bar{p}$ system has total transverse momentum close to 0. The neutrino transverse momentum p_T^{ν} is calculated at each step of the fit, using the fitted values of lepton, jet, and unclustered transverse energies:

$$\mathbf{p}_T^{\nu} = -\left(\mathbf{p}_T^{\ell} + \sum \mathbf{p}_T^{\mathrm{jet}} + \mathbf{p}_T^{\mathrm{UE}}\right). \tag{2}$$

The mass of the neutrino is fixed at zero, and the longitudinal momentum, p_z^{ν}, is a free (unconstrained) parameter in the fit. The initial value of p_z^{ν} is calculated using the initial value of the lepton four-vector and the initial p_T^{ν}, assuming that they arise from a W boson at the nominal pole mass. Since these conditions yield a quadratic equation, there are in general two solutions for the p_z^{ν}; a separate χ^2 fit is done with each solution used as the initial value of p_z^{ν}. When the solutions are imaginary, the real part $\pm$ 20 GeV are the two values of p_z^{ν} used to initialize the fit.

Given the inputs described above, the event-by-event fit for the reconstructed top-quark mass proceeds as follows. MINUIT is used to minimize a χ^2, where m_t^{reco} is a free parameter. For each event, the χ^2 is minimized once for each possible way of assigning the leading four jets to the four quarks from the $t\bar{t}$ decay. Since the two W daughter jets are indistinguishable in the χ^2 expression, the number of permutations is $4!/2 = 12$. In addition, there are two solutions for the initial value of the neutrino longitudinal momentum, so the minimization is performed a total of 24 times for each event. When b tags are present, permutations that assign a tagged jet to a light quark at parton level are rejected. In the case of single-tagged events, the number of allowed permutations is six, and for double-tagged events, it is two. In the rare cases when an event has three b tags, two of the tagged jets must be assigned to b quarks. We use the reconstructed top-quark mass from the permutation with the lowest χ^2 after minimization.

The χ^2 expression has terms for the uncertainty on the measurements of jet, lepton, and unclustered energies, as well as terms for the kinematic constraints

applied to the system:

$$\chi^2 = \sum_{i=\ell,4\text{jets}} \frac{(p_T^{i,\text{fit}} - p_T^{i,\text{meas}})^2}{\sigma_i^2} + \sum_{j=x,y} \frac{(p_j^{\text{UE,fit}} - p_j^{\text{UE,meas}})^2}{\sigma_{\text{UE}}^2} + \\ + \frac{(M_{\ell\nu} - M_W)^2}{\Gamma_W^2} + \frac{(M_{jj} - M_W)^2}{\Gamma_W^2} + \frac{(M_{b\ell\nu} - m_t^{\text{reco}})^2}{\Gamma_t^2} + \\ + \frac{(M_{bjj} - m_t^{\text{reco}})^2}{\Gamma_t^2}. \quad (3)$$

The first term constrains the p_T of the lepton and four leading jets to their measured values within their assigned uncertainties; the second term does the same for both transverse components of the unclustered energy. In the remaining four terms, the quantities $M_{\ell\nu}$, M_{jj}, $M_{b\ell\nu}$, and M_{bjj} refer to the invariant mass of the sum of the four-vectors denoted in the subscripts. For example, $M_{\ell\nu}$ is the invariant mass of the sum of the lepton and neutrino four-vectors. M_W is the pole mass of the W boson, 80.42 GeV/c^2 [25], and m_t^{reco} is the free parameter for the reconstructed top-quark mass used in the minimization. M_{jj} is a quantity computed in the kinematic fit, and should not be confused with m_{jj}, the measured dijet mass used to constrain JES. The fit is initialized with $m_t^{\text{reco}} = 175$ GeV/c^2. Γ_W and Γ_t are the total width of the W boson and the top quark. Γ_W is 2.12 GeV [25], while for the top quark we assume a width of $\Gamma_t = 1.5$ GeV/c^2. Thus these terms provide constraints such that the W masses come out correctly, and the t and $\bar{t}$ masses come out the same (modulo the Breit–Wigner distribution, here modeled by a Gaussian, in both cases).

The jet-quark assignment (and p_z^ν solution) with the lowest χ^2 after minimization is selected for each event. The χ^2 of this combination is denoted χ^2_{min} (or just χ^2 when the context is unambiguous), and the requirement $\chi^2_{\text{min}} < 9$ is imposed. The expected statistical uncertainty on the top-quark mass does not change much over a wide range of the value of the cut, even when it is varied independently for the four event types. The value of the cut chosen is close to the minimum of expected top-quark mass uncertainty.

The dijet masses used to constrain JES in the same data sample used to reconstruct the observed top-quark mass are calculated, with the exception that there is no χ^2 requirement on the jet-quark assignments under consideration. The imposition of the χ^2 requirement would impose a bias in the dijet masses being considered and therefore reduce the sensitivity of the dijet mass distribution to JES. We calculate the dijet masses directly from the measured jet four-vectors without using a kinematic fit and considering all jet-quark assignments in each event for any of the leading 4 jets that are not b-tagged. The Monte Carlo studies have shown that the sensitivity of the dijet mass distribution to the JES parameter

is maximized by considering all dijet mass combinations that do not involve a b-tagged jet in each event. The number of possible assignments ranges from one (for events with two b tags) to six (for events with no b tags).

Typical reconstructed top-quark mass distributions for signal Monte Carlo ($M_{\rm top} = 178$ GeV/c^2) are shown for the four event categories as the light histograms in Fig. 4. Each event in the sample that passes both event selection and the χ^2 cut contributes exactly one entry to these histograms. The distributions peak near the generated mass of 178 GeV/c^2. But there is not an exact correspondence between the generated mass and the mean or peak position of the reconstructed mass. Differences can arise when ISR/FSR jets are selected instead of the $t\bar{t}$ decay products; even with the correct jets, the fit may choose the wrong jet-quark assignment. In particular, the broader shape, beneath the relatively sharp peak at 178 GeV/c^2, comprises events where an incorrect permutation has been chosen in the fit. The dark histograms in the same figure show the reconstructed

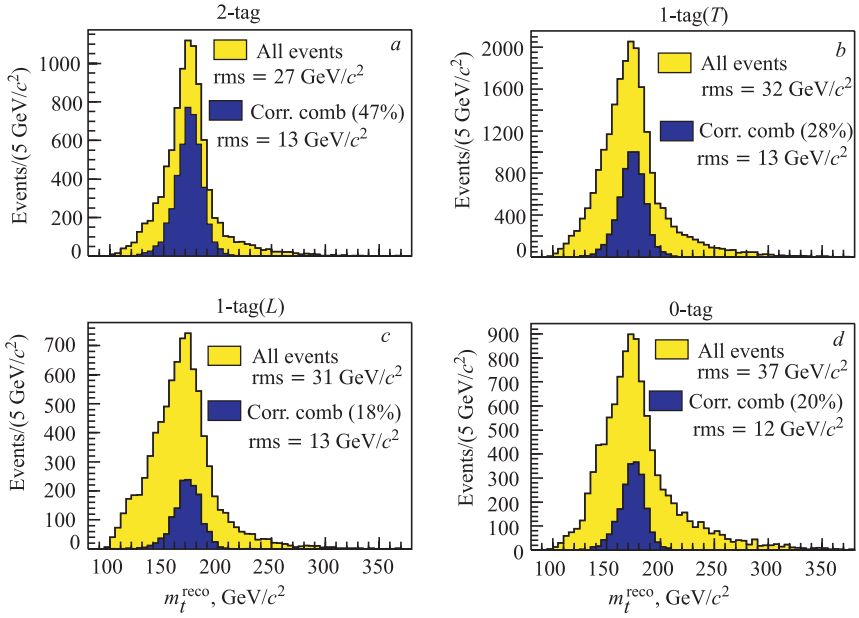

Fig. 4. The light histograms show the reconstructed top-quark mass distribution for the 178 GeV/c^2 HERWIG $t\bar{t}$ sample at the nominal jet energy scale. Overlaid are darker histograms of the reconstructed mass distributions using the subset of events for which the leading four jets are matched (within $\Delta R = 0.4$) to the four quarks from the $t\bar{t}$ decay and the correct jet-quark assignment has the lowest χ^2. Distributions are shown for 2-tag (*a*), 1-tag(T) (*b*), 1-tag(L) (*c*), and 0-tag (*d*) events

mass distributions for events where the four leading jets correspond to the four quarks from $t\bar{t}$ decay, and where the correct jet-quark assigment is chosen by the fit. These histograms have much smaller tails than the overall distributions, and account for 47% of the 2-tagsample, 28% of the 1-tag(T)sample, 18% of the 1-tag(L), and 20% of the 0-tag category.

2.2. Dilepton Methods. Reconstruction of the top-quark mass from dilepton events involves an underconstrained system because there is no one-to-one correspondence between observables and all decay particles. For lepton + jets decays, the two components of $\not\!\!E_T$ generated by the single neutrino, along with other assumptions about the $t\bar{t}$ event (e.g., equal masses for the t and $\bar{t}$ quarks, and invariant masses of the $\ell\nu$ and $q\bar{q}'$ systems equal to the W mass) are enough to allow a kinematically overconstrained fit. For dilepton $t\bar{t}$ events, in contrast, the measured $\not\!\!E_T$ is due to two neutrinos, so that the decay assumptions are insufficient to constrain the event.

Specifically, for each $t\bar{t}$ event, the kinematics are fully specified by 24 quantities: the four-momenta of the six final-state particles. Twelve three-momentum components of the two b quarks and two leptons are measured by the detector, along with the two components of $\not\!\!E_T$. The four mass values of the final state b quarks and leptons are known, while the two neutrinos are assumed to be massless. Making three additional assumptions about the $t\bar{t}$ and W boson decays:

$$m(b\ell^+\nu) = m(\bar{b}\ell^-\bar{\nu}), \tag{4}$$

$$m(\ell^+\nu) = m(W^+), \tag{5}$$

$$m(\ell^-\bar{\nu}) = m(W^-) \tag{6}$$

results in only 23 measured, known, or assumed components of the system. Therefore, the top-quark mass cannot be directly reconstructed from $t\bar{t}$ dilepton decays, but requires one additional kinematic assumption to constrain the system.

In practice, for each event one integrates over an undetermined kinematical variable to obtain distributions giving the relative likelihood of different values of the top-quark mass. The three mass analyses are distinguished by different choices of kinematical variable, different methods for determining the likelihood of each top-quark mass, and different approaches to distilling the resulting information into one top-quark mass per event. This section describes each technique in turn. We model the $t\bar{t}$ decay kinematics and optimize each method over a large range of top-quark masses, using HERWIG Monte Carlo simulation with CTEQ5L [26] parton distribution functions. Potential bias in reconstructed top-quark mass of each method is accounted for by comparing the measured results with top-quark mass templates derived using the simulation.

2.2.1. Neutrino ϕ Weighting Method (PHI). A first procedure for analyzing $t\bar{t}$ dilepton decays, referred to as the Neutrino ϕ Weighting Method (PHI) [5,7], most closely resembles the Run-I lepton + jets template analysis [27]. Introducing

additional assumptions about the azimuthal angle ϕ of the final-state neutrinos, this method reconstructs dilepton decays through the minimization of a chi-square functional (χ^2) to arrive at a single top-quark mass for each event. The PHI method uses the 340 pb^{-1} DIL selection sample.

The χ^2 functional to be minimized takes the form:

$$\chi^2 = \sum_{\ell=1}^{2} \frac{(p_T^\ell - \widetilde{p_T^\ell})^2}{{\sigma_{p_T}^\ell}^2} + \sum_{j=1}^{2} \frac{(p_T^j - \widetilde{p_T^j})^2}{{\sigma_{p_T}^j}^2} + \sum_{i=x,y} \frac{(\mathrm{UE}^i - \widetilde{\mathrm{UE}^i})^2}{{\sigma_{\mathrm{UE}}^i}^2} + \\ + \frac{(m_{\ell_1\nu_1} - m_W)^2}{\Gamma_W^2} + \frac{(m_{\ell_2\nu_2} - m_W)^2}{\Gamma_W^2} + \\ + \frac{(m_{j_1\ell_1\nu_1} - \widetilde{m_t})^2}{\Gamma_t^2} + \frac{(m_{j_2\ell_2\nu_2} - \widetilde{m_t})^2}{\Gamma_t^2}. \quad (7)$$

The first term sums over the primary lepton transverse momenta p_T^ℓ, with detector resolutions for the electrons and muons taken to be [10]:

$$\frac{\sigma_{p_T}^e}{p_T^e} = \sqrt{\frac{0.135^2}{p_T^e} + 0.02^2}, \quad (8)$$

$$\frac{\sigma_{p_T}^\mu}{p_T^\mu} = 0.0011 p_T^\mu. \quad (9)$$

The second χ^2 term sums over the transverse momenta p_T^j of the two leading jets, which are further corrected for underlying event and out-of-cone energy, and have a p_T- and η-dependent detector resolution $\sigma_{p_T}^j$ derived from simulation. The quantity UE (with uncertainty σ_{UE}) in the third χ^2 term denotes the unclustered energy in the calorimeter, summed over $(i = x, y)$ directions, which is not associated with a lepton or leading jet calorimeter cluster, but includes any additional jets with $E_T > 8$ GeV/c^2 and $|\eta| < 2.5$. The quantities $m_{\ell\nu}$ and $m_{j\ell\nu}$ in Eq. (7) refer to the reconstructed invariant masses of the W boson and top-quark decay products, respectively. Variables with a tilde refer to the output of the minimization procedure. The quantity $\widetilde{m_t}$ is the fit parameter returning the reconstructed top-quark mass for the combination being considered.

To resolve the neutrino momentum used in the W and top decay constraints of Eq. (7), two additional assumptions are needed. Assuming values for both neutrino azimuthal angles ($\phi_{\nu 1}, \phi_{\nu 2}$), the transverse momenta of the neutrinos are linked through the measured $\not\!\!E_T$ by:

$$\begin{aligned} p_T^{\nu 1} \cos(\phi_{\nu 1}) + p_T^{\nu 2} \cos(\phi_{\nu 2}) &= \not\!\!E_x, \\ p_T^{\nu 1} \sin(\phi_{\nu 1}) + p_T^{\nu 2} \sin(\phi_{\nu 2}) &= \not\!\!E_y \end{aligned} \quad (10)$$

leading to the solutions:

$$
\begin{aligned}
p_x^{\nu 1} \equiv p_T^{\nu 1}\,\cos(\phi_{\nu 1}) &= \frac{\not\!\!E_x\,\sin(\phi_{\nu 2}) - \not\!\!E_y\,\cos(\phi_{\nu 2})}{\sin(\phi_{\nu 2}-\phi_{\nu 1})}\,\cos(\phi_{\nu 1}),\\
p_y^{\nu 1} \equiv p_T^{\nu 1}\,\sin(\phi_{\nu 1}) &= \frac{\not\!\!E_x\,\sin(\phi_{\nu 2}) - \not\!\!E_y\,\cos(\phi_{\nu 2})}{\sin(\phi_{\nu 2}-\phi_{\nu 1})}\,\sin(\phi_{\nu 1}),\\
p_x^{\nu 2} \equiv p_T^{\nu 2}\,\cos(\phi_{\nu 2}) &= \frac{\not\!\!E_x\,\sin(\phi_{\nu 1}) - \not\!\!E_y\,\cos(\phi_{\nu 1})}{\sin(\phi_{\nu 1}-\phi_{\nu 2})}\,\cos(\phi_{\nu 2}),\\
p_y^{\nu 2} \equiv p_T^{\nu 2}\,\sin(\phi_{\nu 2}) &= \frac{\not\!\!E_x\,\sin(\phi_{\nu 1}) - \not\!\!E_y\,\cos(\phi_{\nu 1})}{\sin(\phi_{\nu 1}-\phi_{\nu 2})}\,\sin(\phi_{\nu 2}).
\end{aligned}
\tag{11}
$$

Performing the χ^2 minimization of Eq. (7) on all allowed values of neutrino ϕ creates a set of solutions in the $(\phi_{\nu 1}, \phi_{\nu 2})$ plane. In practice, only points in the quadrant $(0 < \phi_{\nu 1} < \pi, 0 < \phi_{\nu 2} < \pi)$ must be sampled, since identical neutrino momentum components from Eq. (11) occur for the four points $(\phi_{\nu 1}, \phi_{\nu 2})$, $(\phi_{\nu 1} + \pi, \phi_{\nu 2})$, $(\phi_{\nu 1}, \phi_{\nu 2} + \pi)$, and $(\phi_{\nu 1} + \pi, \phi_{\nu 2} + \pi)$. Since $p_T^{\nu 1,\nu 2}$ must be positive by definition, and will only change sign by adding π to $\phi_{\nu 1,\nu 2}$, only one of the four points represents a physical solution. Solutions from other points are unphysical and can be interpreted as «mirror reflections» of the physical solution.

A grid of 12×12 points in the $(\phi_{\nu 1}, \phi_{\nu 2})$ plane is chosen, in a manner which avoids points where $\sin(\phi_{\nu 1} - \phi_{\nu 2}) = 0$ and Eq. (11) becomes undefined. At each point, eight solutions exist due to the two-fold ambiguity in longitudinal momentum for each neutrino and the two possible lepton-jet combinations. *Thus,*

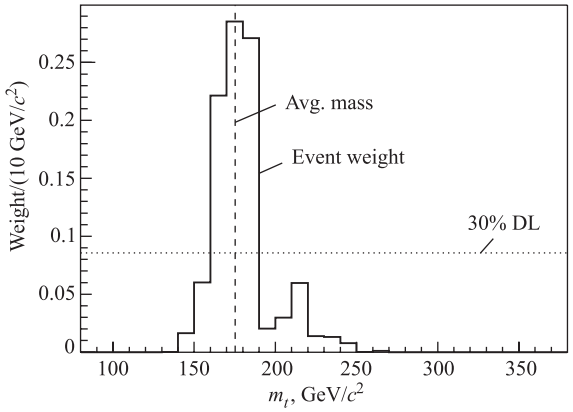

Fig. 5. Binned weight distribution from the PHI method for a HERWIG Monte Carlo $t\bar{t}$ event with $m_t = 170$ GeV/c^2, showing the resulting average mass for bins above the 30% discrimination level (DL)

for each event, 1152 minimizations of Eq. (7) are performed, each returning an output χ^2 and reconstructed top-quark mass $\tilde{m}_t$. The minimal value for χ^2 among the eight possible solutions at each point is retained, reducing each event to an array of 144 χ^2_{ij} and $m_{t_{ij}}$ values, where $(i = 1, 12; j = 1, 12)$ refer to the $(\phi_{\nu 1}, \phi_{\nu 2})$ grid points. Each point is weighted by its returned χ^2 value according to:

$$w_{ij} = \frac{\exp\left(-\chi^2_{ij}/2\right)}{\sum\limits_{i=1}^{12}\sum\limits_{j=1}^{12}\exp\left(-\chi^2_{ij}/2\right)} \tag{12}$$

to create a probability density distribution normalized to unity.

To arrive at a single top-quark mass value per event, the reconstructed mass values $m_{t_{ij}}$ of the array are averaged, using the weights derived from Eq. (12). The sensitivity to the top-quark mass is enhanced by averaging only points with a weight at least 30% that of the most probable value in the probability density distribution. Figure 5 shows the results of the PHI method applied to a HERWIG Monte Carlo $t\bar{t}$ event with $m_t = 170$ GeV/c^2.

2.2.2. Neutrino Weighting Algorithm (NWA). The second method for estimating the top-quark mass from dilepton events uses the Neutrino Weighting Algorithm (NWA) [28]. In Run-I at the Tevatron, the NWA method was one of two techniques used by DØ [29], and was employed by CDF [27] to measure the top-quark mass. The method therefore provides a baseline for CDF Run-II measurements, and is applied to the 360 pb^{-1} LTRK event sample. The strategy of the algorithm is to solve for the neutrino and antineutrino momenta, independently of the measured missing energy, by making additional assumptions about the $t\bar{t}$ decay. The neutrino/antineutrino solutions are then compared with the measured $\not\!\!E_T$ through a weight function in order to create a probability distribution for the event as a function of top-quark mass.

The NWA weight function is constructed as follows. Values for the top-quark and W-boson masses are assumed, the pseudorapidities of the neutrino and antineutrino, and the lepton-jet pairings are associated with the top/antitop decays. The energy-momentum conservation is applied to the top-quark decay and obtain up to two possible solutions for the 4-momentum ($\boldsymbol{\nu}$) of the neutrino. This procedure is repeated on the antitop decay, resulting in up to four possible pairs of neutrino–antineutrino solutions ($\boldsymbol{\nu}, \bar{\boldsymbol{\nu}}$). For each of the four solutions a probability (weight, w_i) is assigned that describes the observed missing transverse energy components $\not\!\!E_x$ and $\not\!\!E_y$ within their uncertainties σ_x and σ_y, respectively:

$$w_i = \exp\left(-\frac{(\not\!\!E_x - p^{\nu}_x - p^{\bar{\nu}}_x)^2}{2\sigma_x^2}\right)\exp\left(-\frac{(\not\!\!E_y - p^{\nu}_y - p^{\bar{\nu}}_y)^2}{2\sigma_y^2}\right). \tag{13}$$

$\sigma_x = \sigma_y = 15$ GeV is used, which is obtained from $t\bar{t}$ Monte Carlo simulation generated with $m_t = 178$ GeV/c^2. In practice, however, the performance of the algorithm is insensitive to the particular choice of $\not\!\!E_T$ resolution.

Given the assumed top-quark mass and assumed neutrino η values, any of the four solution pairs $(\boldsymbol{\nu}, \bar{\boldsymbol{\nu}})$ have *a priori* equal probability. The sum over the four weights is:

$$w(m_t, \eta_\nu, \eta_{\bar{\nu}}, \ell\text{–jet}) = \sum_{i=1}^{4} w_i. \tag{14}$$

Not knowing which are the true neutrino η's in our event, the above steps are repeated for many possible $(\eta_\nu, \eta_{\bar{\nu}})$ pairs. As seen in the upper plots of Fig. 6, Monte Carlo $t\bar{t}$ simulation indicates that the neutrino η's are uncorrelated, and follow a Gaussian distribution centered at zero with a width near one. Since the

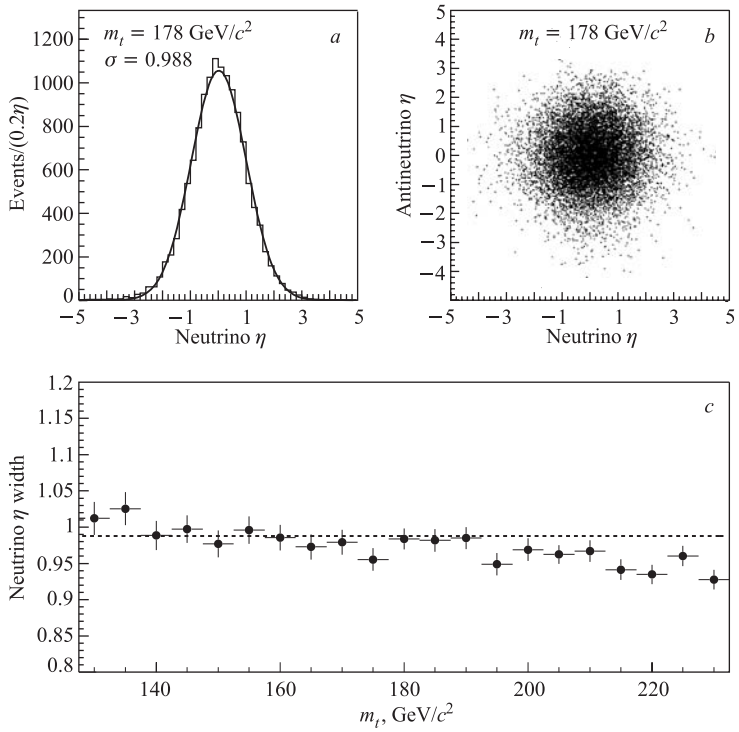

Fig. 6. Neutrino η distribution with Gaussian fit (*a*) and neutrino vs. antineutrino η (*b*) from a HERWIG $t\bar{t}$ sample with $m_t = 178$ GeV/c^2. Figure *c* shows η width as a function of generated top-quark mass, compared with fit value at $m_t = 178$ GeV/c^2 (horizontal line)

neutrino η width varies little with top-quark mass (as shown in Fig. 6, *c*), one assumes a constant width for all top-quark masses corresponding to the value of 0.988 obtained from the $m_t = 178$ GeV/c^2 sample. To ensure symmetry and smoothness, the neutrino η distributions are scanned from -3 to $+3$ in steps of 0.1, and each $(\eta_\nu, \eta_{\bar{\nu}})$ pair is assigned a probability of occurrence $P(\eta_\nu, \eta_{\bar{\nu}})$ derived from a Gaussian of width 0.988. Each trial $(\eta_\nu, \eta_{\bar{\nu}})$ pair contributes to the event according to its weight (Eq. (14)) and probability of occurrence, $P(\eta_\nu, \eta_{\bar{\nu}})$:

$$w(m_t, \ell\text{–jet}) = \sum_{\eta_\nu, \eta_{\bar{\nu}}} P(\eta_\nu, \eta_{\bar{\nu}}) w(m_t, \eta_\nu, \eta_{\bar{\nu}}, \ell\text{–jet}). \tag{15}$$

Since b jets are not distinguished from $\bar{b}$ jets, both possible lepton-jet pairings are summed. Thus, the final weight becomes a function only of the top-quark mass, after integrating over all other unknowns:

$$W(m_t) = \sum_{\ell^+\text{–jet}_1}^{\ell^+\text{–jet}_2} w(m_t, \ell\text{–jet}), \tag{16}$$

m_t is scanned from 80 to 380 GeV/c^2 in steps of 1 GeV/c^2. Figure 7 shows the resulting normalized weight distribution from Eq. (16) after applying the NWA method to a HERWIG Monte Carlo $t\bar{t}$ event, with a simulated top-quark mass of 170 GeV/c^2. One indicative top-quark mass is chosen for each event, selecting the most probable value (MPV) of the weight distribution as that which best explains the event as a $t\bar{t}$ dilepton decay.

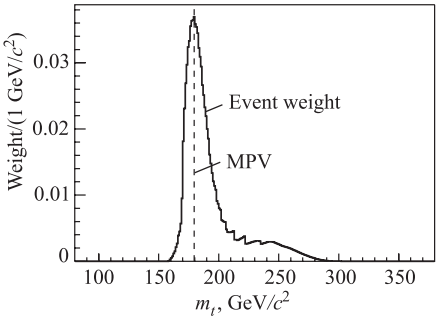

Fig. 7. NWA weight distribution as a function of top-quark mass hypothesis (from Eq. (16)) for a HERWIG Monte Carlo $t\bar{t}$ event with $m_t = 170$ GeV/c^2. The vertical line denotes the most probable value (MPV) of m_t chosen by the method

For a given event, there exists a small probability that the kinematics of the decay will fail to produce a solution for any scanned top-quark mass. This efficiency for finding a solution is thus an additional event selection criterion. Studies of simulated $t\bar{t}$ dilepton events show that this NWA efficiency for signal is 99.8%, and independent of generated top-quark mass. Applying the NWA method to Monte Carlo background samples shows that the efficiency for finding

a kinematical solution varies between sources, ranging from 94–100%, with an average background efficiency of 96%.

2.2.3. Full Kinematic Analysis (KIN). A third method for determining the top-quark mass in the dilepton channel, called the Full Kinematic Analysis (KIN) [28], is applied to the 340 pb^{-1} DIL selection sample. The KIN method resolves the underconstrained dilepton $t\bar{t}$ decays by introducing an additional equation for the longitudinal momentum of the $t\bar{t}$ system, $p_z^{t\bar{t}}$. With the 6-particle final state constrained, the KIN method solves the resulting kinematic equations numerically to determine the top-quark mass for each event.

Ideally, the quantity $p_z^{t\bar{t}}$ should be determined theoretically and should be virtually independent of the top-quark mass. Studies from Monte Carlo simulation over a range of top-quark masses from 140–200 GeV/c^2 show that $p_z^{t\bar{t}}$ has a Gaussian behavior, with a mean of zero and a width near 180 GeV/c.

Using the measured momenta of the b quarks and leptons, the two components of the measured $\not\!\!E_T$, and assumptions about the six final-state particle masses, the additional constraint on $p_z^{t\bar{t}}$, along with constraints on the W and $t\bar{t}$ decays, lead to the following set of kinematic equations:

$$\begin{gathered} p_x^{\nu} + p_x^{\bar{\nu}} = \not\!\!E_x\,, \quad p_y^{\nu} + p_y^{\bar{\nu}} = \not\!\!E_y\,, \quad p_z^{t} + p_z^{\bar{t}} = 0 \pm 180 \text{ GeV}/c, \\ m_t = m_{\bar{t}}, \quad m_{W^{\pm}} = 80.4 \text{ GeV}/c^2, \\ \mathbf{p}_b + \mathbf{p}_{W^+} = \mathbf{p}_t, \quad \mathbf{p}_{\bar{b}} + \mathbf{p}_{W^-} = \mathbf{p}_{\bar{t}}, \\ \mathbf{p}_{l^+} + \mathbf{p}_{\nu} = \mathbf{p}_{W^+}, \quad \mathbf{p}_{l^-} + \mathbf{p}_{\bar{\nu}} = \mathbf{p}_{W^-}, \end{gathered} \tag{17}$$

which have two solutions determined through an iterative procedure. If solutions cannot be found by using the above assumptions for the top and bottom quark masses, these requirements are relaxed, and the solutions are accepted where $m_{W^{\pm}} = (80.4 \pm 3.0)$ GeV/c^2 and $m_t = (m_{\bar{t}} \pm 2.0)$ GeV/c^2. If no solutions are found after relaxing the mass requirements, the event is rejected.

The iterative procedure employed, Newton's method [30], solves equations of the form $f(x) = 0$. The method requires an initial guess for x which is reasonably close to the true root. The local derivative $f'(x)$ is then computed and extrapolated to zero, providing a better approximation for the root. This procedure is repeated according to:

$$x^{n+1} = x^n - \frac{f(x^n)}{f'(x^n)} \tag{18}$$

until a satisfactory solution is found. The method is extended to a system of k equations $F(\mathbf{x}) = f_i(\mathbf{x})$ by determining the $k \times k$ Jacobian matrix $J_F^{ij}(\mathbf{x}) = \dfrac{\partial f_i(\mathbf{x})}{\partial x_j}$, where $(i = 1, k; j = 1, k)$. In actuality, the method solves the linear equations:

$$J_F(\mathbf{x}^n)(\mathbf{x}^{n+1} - \mathbf{x}^n) = -F(\mathbf{x}^n) \tag{19}$$

for the unknown $\mathbf{x}^{n+1} - \mathbf{x}^n$, in order to avoid having to compute the inverse of $J_F(\mathbf{x}^n)$.

Applying Newton's method to the $t\bar{t}$ decay system of Eq. (17), the first of two pairs of quadratic solutions are determined for the neutrino momentum according to the following set of three equations:

$$f_1(p_x^{\nu_1}, p_y^{\nu_1}, p_z^{\nu_1}) \equiv (E_{l_1} + E_{\nu_1})^2 - (\mathbf{p}_{l_1} + \mathbf{p}_{\nu_1})^2 - m_W^2 = 0, \tag{20}$$

$$f_2(p_x^{\nu_1}, p_y^{\nu_1}, p_z^{\nu_1}) \equiv (E_{l_2} + E_{\nu_2})^2 - (\mathbf{p}_{l_2} + \mathbf{p}_{\nu_2})^2 - m_W^2 = 0, \tag{21}$$

$$\begin{aligned} f_3(p_x^{\nu_1}, p_y^{\nu_1}, p_z^{\nu_1}) \equiv (E_{l_1} + E_{\nu_1} + E_{b_1})^2 - (\mathbf{p}_{l_1} + \mathbf{p}_{\nu_1} + \mathbf{p}_{b_1})^2 - \\ - (E_{l_2} + E_{\nu_2} + E_{b_2})^2 + (\mathbf{p}_{l_2} + \mathbf{p}_{\nu_2} + \mathbf{p}_{b_2})^2 = 0 \end{aligned} \tag{22}$$

from which the full kinematic chain is reconstructed, and the top-quark mass are calculated. The second quadratic solution for neutrino momentum $\mathbf{p}'_{\nu_1} \equiv \mathbf{p}_{\nu_1} + \mathbf{X}$ satisfies the following set of equations:

$$f_1(x_1, x_2, x_3) \equiv \sqrt{m_W^2 + (\mathbf{p}_{W_1} + \mathbf{X})^2} - E_{l_1} - \sqrt{(\mathbf{p}_{\nu_1} + \mathbf{X})^2} = 0, \tag{23}$$

$$f_2(x_1, x_2, x_3) \equiv \sqrt{m_W^2 + (\mathbf{p}_{W_2} - \mathbf{X})^2} - E_{l_2} - \sqrt{(\mathbf{p}_{\nu_2} - \mathbf{X})^2} = 0, \tag{24}$$

$$\begin{aligned} f_3(x_1, x_2, x_3) \equiv \sqrt{(\sqrt{m_W^2 + (\mathbf{p}_{W_1} + \mathbf{X})^2} + E_{b_1})^2 - (\mathbf{p}_{t_1} + \mathbf{X})^2} - \\ - \sqrt{(\sqrt{m_W^2 + (\mathbf{p}_{W_2} - \mathbf{X})^2} + E_{b_2})^2 - (\mathbf{p}_{t_2} - \mathbf{X})^2} = 0 \end{aligned} \tag{25}$$

from which a second pair of top-quark mass solutions is found. Since there are two possible combinations of b-quark jets and leptons, there are a total of eight possible solutions for the top-quark mass.

In order to incorporate the large range of possible $p_z^{t\bar{t}}$ values about the mean of zero, as well as the finite resolutions of the measured momenta and $\not{E}_T$, the above procedure is repeated 10,000 times for each solution set. For each repetition, the value of $p_z^{t\bar{t}}$ is drawn from a Gaussian distribution with zero mean and width of 180 GeV/c. The jet energies and $\not{E}_T$ are similarly smeared by Gaussians according to their estimated resolutions, while the relatively better resolutions on the measured jet angles and lepton momenta are ignored. Kinematic reconstruction of the smeared events results in a distribution of possible top-quark masses for a given event (consistent with the measured kinematic characteristics of the event and the measurement uncertainties). The most probable value (MPV) of a spline fit to this mass distribution is then taken as the «raw top-quark mass» for a given solution.

The KIN method then selects a single «raw top-quark mass» from the eight possible solutions as follows. Of the four possible solutions for each lepton-jet pairing, we choose that with the smallest effective mass of the $t\bar{t}$ system.

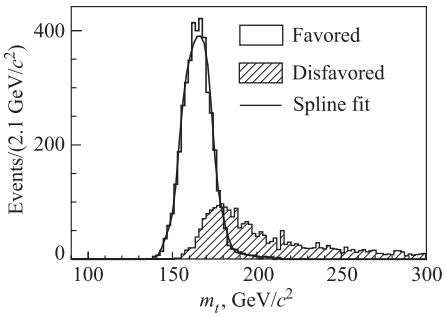

Fig. 8. Smeared top-quark mass distributions of the «favored» and «disfavored» lepton-jet pairings from the KIN method applied to a HERWIG Monte Carlo $t\bar{t}$ event with $m_t = 170$ GeV/c^2. Also shown for the «favored» pair is the spline fit used to select the top-quark mass for a given solution

Based on simulated events at $m_t = 178$ GeV/c^2, this particular mass solution is the closest to the generator-level top-quark mass for approximately 84% of the events. The smeared mass distributions of the remaining two possible solutions (due to the two lepton-jet pairings) are then compared, as shown in Fig. 8 for an example simulation event. Method chooses the lepton-jet pair which produces the largest number of entries (i.e., the fewest number of rejections) in the smeared distribution. The mass solution from this kinematically «favored» pair is found to be the closest to the generated top-quark mass for about 70% of events. In this manner, the KIN method returns a single top-quark mass for each $t\bar{t}$ dilepton event.

3. LIKELIHOOD PROCEDURE FOR TEMPLATE METHODS

The independent template measurement techniques described in Sec. 2 produce a single top-quark mass for each event in their corresponding data samples, which are mixtures of $t\bar{t}$ signal and background events. To arrive at a final top-quark mass measurement, these data events are compared with probability density functions (p.d.f.'s) for signal and background within a likelihood minimization.

The p.d.f.'s are developed from template mass distributions created by applying the (l + jets) template method as well as dilepton NWA, KIN, and PHI methods to simulated $t\bar{t}$ signal and background samples, which are then parameterized. For the NWA and PHI methods, this parameterization uses a combination of Gaussian and gamma distribution terms. Similarly, the KIN method parameterization contains a Gaussian term in conjunction with an approximate Landau distribution.

The likelihood procedure will be shown taking as example the dilepton PHI method.

3.1. Template Construction. For the signal, the $t\bar{t}$ dilepton events generated with HERWIG Monte Carlo simulation are used for top-quark masses from 130 to 230 GeV/c^2 in 5 GeV/c^2 increments. The CTEQ5L [26] Structure Functions are used to model the momentum distribution of the initial state partons. The

signal templates obtained from this simulation are parameterized as the sum of a Gaussian and a gamma distribution. This parameterization gives the signal p.d.f, $P_s(m; m_t)$, representing the probability of reconstructing a top-quark mass m when the true mass is m_t:

$$P_s(m; m_t) = \alpha_5 \frac{\alpha_2^{1+\alpha_1}}{\Gamma(1+\alpha_1)}(m-\alpha_0)^{\alpha_1} \exp\left(-\alpha_2(m-\alpha_0)\right) + \\ + (1-\alpha_5)\frac{1}{\alpha_4\sqrt{2\pi}} \exp\left(-\frac{(m-\alpha_3)^2}{2\alpha_4^2}\right). \quad (26)$$

The six parameters α_i in Eq. (26) are assumed to be linearly dependent on the generated top-quark mass, such that we in fact perform a 12-parameter fit for p_i on all templates simultaneously, with:

$$\alpha_i = p_i + (m_t - 175 \text{ GeV}/c^2)\, p_{i+6}. \quad (27)$$

Figure 9 shows representative signal templates with the corresponding parameterized fitting function.

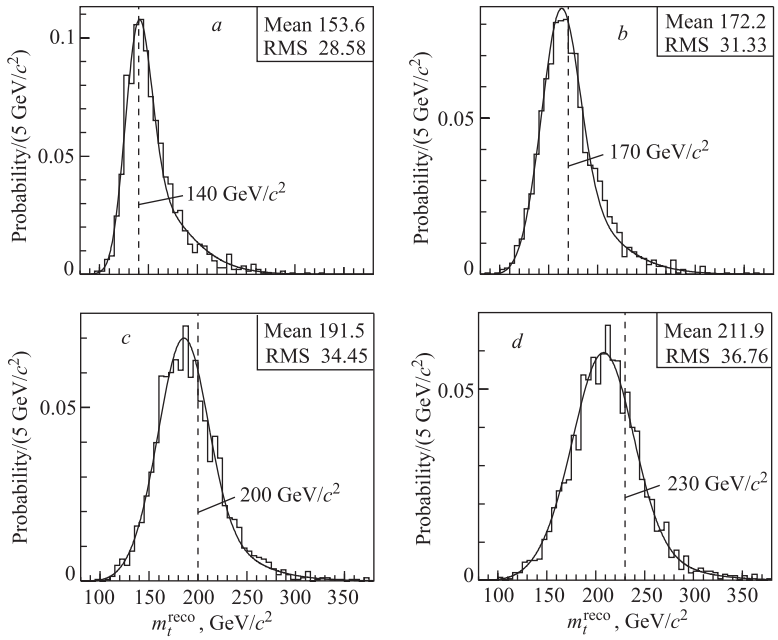

Fig. 9. Example signal templates as a function of the reconstructed top-quark mass, from the PHI method applied to simulated signal samples at top-quark masses of 140 (*a*), 170 (*b*), 200 (*c*), and 230 GeV/c^2 (*d*). Overlaid are the parameterized fitting functions using Eq. (26). The vertical line indicates the generated top-quark mass

One can see for all template methods, the mean of the signal template lies above the generated top-quark mass for the $m_t = 140$ GeV/c^2 sample, but moves below the generated value for higher mass samples (Fig. 9).

For the background events, we create one representative background template by adding the individual templates from each background source according to their expected yields from Table 3. The templates from the various background processes are reconstructed from fully simulated Monte Carlo samples: the Drell–Yan events from PYTHIA, the $W(\to \ell\nu) +$ jets fakes from ALPGEN + HERWIG simulation of $W(\to e\nu) + 3$ partons, and the diboson from PYTHIA and ALPGEN + HERWIG [23, 24]. In combining these sources for each mass measurement technique, the measured efficiencies for finding a mass solution for each simulated background source are taken into account. The background p.d.f.'s ($P_b(m)$) are obtained by fitting the combined background template with a functional form identical to that used for the signal templates, but with fitted parameters independent of true top-quark mass m_t.

The resulting mass templates for the three background sources, along with the combined background template and parameterized fit, are plotted in Fig. 10.

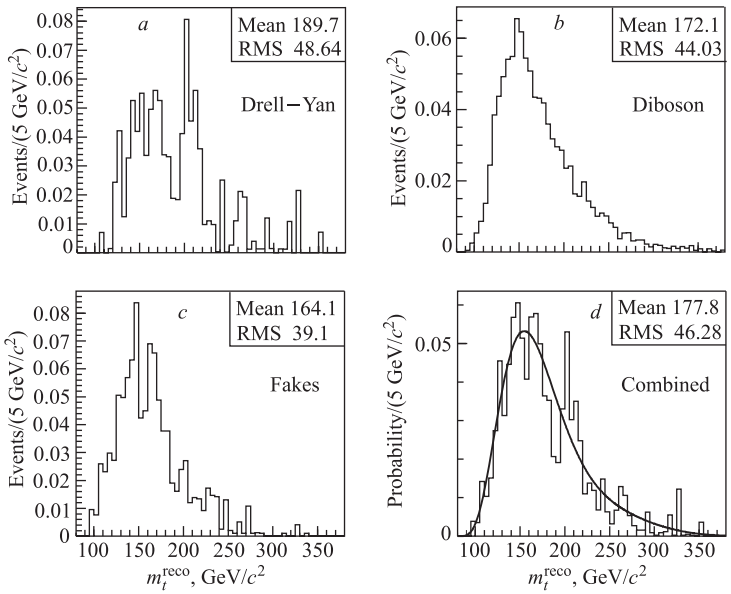

Fig. 10. Reconstructed top-quark mass templates for the Drell–Yan (*a*), Diboson (*b*), and Fakes (*c*) background sources using the PHI method, along with the combined (*d*) background template and associated fitted probability density function. Background sources are normalized to the expected contribution in the 340 pb^{-1} DIL sample

3.2. Likelihood Minimization. The final step for each template analysis is the determination of a representative top-quark mass from the data sample by performing a likelihood fit and minimization. The likelihood function finds the probability that our data are described by an admixture of background events and dilepton $t\bar{t}$ decays with a certain top-quark mass. The top-quark mass values returned by the particular mass measurement technique applied to the data sample are used as input, and the parameterized probability density functions of the signal and background templates derived from simulation.

The total likelihood takes the form:

$$\mathcal{L}(m_t) = \mathcal{L}_{\text{shape}}(m_t) \times \mathcal{L}_{n_b}, \tag{28}$$

where

$$\mathcal{L}_{\text{shape}}(m_t) = \frac{\mathrm{e}^{-(n_s+n_b)}(n_s+n_b)^N}{N!} \prod_{i=1}^{N} \frac{n_s P_s(m_i; m_t) + n_b P_b(m_i)}{n_s + n_b} \tag{29}$$

and

$$-\ln \mathcal{L}_{n_b} = \frac{(n_b - n_b^{\text{exp}})^2}{2\sigma_{n_b}^2}. \tag{30}$$

A probability that each event (i) looks like a signal and a probability that it looks like background are assigned. The signal and background probabilities are assigned by comparing the measured top-quark mass values m_i from the data with the parameterized signal and background p.d.f.'s P_s and P_b. One finds the probabilities that the likelihood-estimate for the number of background events n_b is consistent with our *a priori* estimate n_b^{exp}, and that the likelihood-estimate for the total number of signal (n_s) and background events is consistent with the observed number of events N. The number of background events is constrained with a Gaussian (of width equal to the expected background uncertainty σ_{n_b}), while the total number of events is constrained with a Poisson term. The true top-quark mass hypothesis (m_t) which minimizes $-\ln(\mathcal{L})$ is retained.

The statistical uncertainty on m_t is given by the difference between the minimization mass result and the mass at $-\ln(\mathcal{L}/\mathcal{L}_{\max}) + 0.5$.

In the NWA and KIN analyses, uncertainty on the top-quark mass from uncertainties in the signal and background template parameterizations (due to limited statistics of the simulated template samples) is estimated and included as a systematic uncertainty. The PHI analysis incorporates this parameterization uncertainty directly into the top-quark mass statistical uncertainty through the addition of the third term to the likelihood function (Eq. (28)):

$$\begin{aligned}\mathcal{L}_{\text{param}} &= \\ &= \exp\left(-0.5\{(\boldsymbol{\alpha}-\boldsymbol{\alpha}_0)^T U^{-1}(\boldsymbol{\alpha}-\boldsymbol{\alpha}_0) + (\boldsymbol{\beta}-\boldsymbol{\beta}_0)^T V^{-1}(\boldsymbol{\beta}-\boldsymbol{\beta}_0)\}\right), \end{aligned} \tag{31}$$

where U and V represent the covariance matrices of the signal and background parameters α and β, respectively.

4. TESTING WITH PSEUDOEXPERIMENTS FOR DILEPTON TEMPLATE METHODS

A large number of simulated data ensembles, or pseudoexperiments are used to check whether the methods for mass measurement described above return the expected top-quark mass. For each generated top-quark mass from 150 to 210 GeV/c^2, we construct a set of pseudoexperiments. Each pseudoexperiment consists of masses drawn randomly from the signal and background mass templates (e.g., Figs. 9 and 10). The numbers of signal and background events in each pseudoexperiment are given by random Poisson fluctuations around the *a priori* estimates. These estimates correspond to a $t\bar{t}$ cross section of 6.1 pb, and are adjusted for the reconstruction efficiency of each method for finding top-quark mass solutions for signal and background events. The likelihood minimization procedure described in the previous section provides a «measured» top-quark mass and statistical uncertainty for each pseudoexperiment.

For example, Fig. 11 shows the results from these pseudoexperiments for the dilepton PHI methods. Figure 11, *a* shows that the measured output top-quark mass tracks the generated input mass. From Fig. 11, *b* we observe that the residual differences between input and output top-quark masses are consistent with zero,

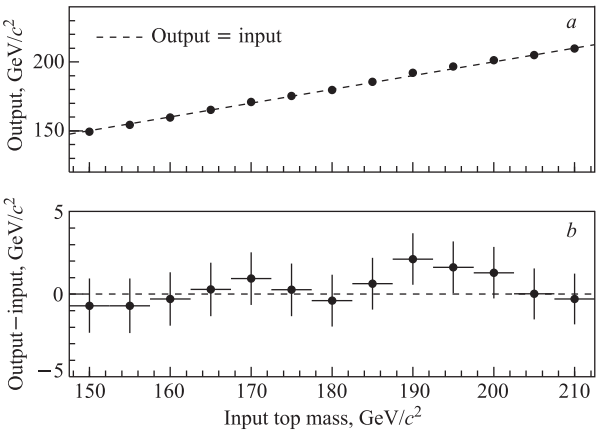

Fig. 11. Results from pseudoexperiment tests of the PHI method. Figure *a* shows the mean of the output (measured) top-quark mass as a function of the input (generated) mass, while Fig. *b* gives the difference between output and input top-quark masses as a function of the input mass

within uncertainties due to the limited statistics of the signal and background mass templates.

In order to check the consistency between the spread in output top-quark mass and the estimated positive (σ_+) and negative (σ_-) statistical uncertainties from the pseudoexperiments, pull distributions are generated according to:

$$\text{pull} \equiv \frac{m_{\text{out}} - m_{\text{in}}}{(\sigma_+ + \sigma_-)/2} \tag{32}$$

for each of the generated samples at different input mass. Figure 12 summarizes the pull mean and width on the example of PHI method as a function of generated top-quark mass, with corresponding uncertainties due to mass template statistics.

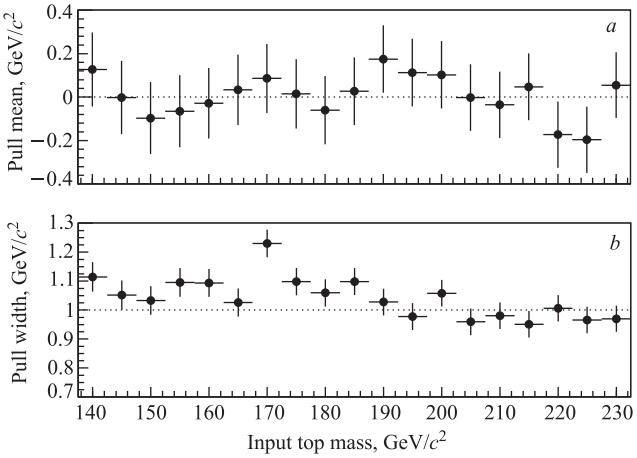

Fig. 12. Summary of pull distributions for the PHI pseudoexperiments, showing the pull mean (*a*) and width (*b*) as a function of generated input top-quark mass, compared with zero mean and unity width (horizontal lines)

Table 4. **Expected signal and background events for the NWA, KIN, and PHI methods applied to the LTRK (360 pb^{-1}) or DIL (340 pb^{-1}) selections, and corresponding to a $t\bar{t}$ cross section of 6.1 pb. Event numbers are adjusted for signal and background reconstruction efficiencies (in parentheses). Also shown is the *a priori* statistical uncertainty on top mass for each method using the $m_t = 178$ GeV/c^2 simulation sample and correcting for underestimation found in pulls (by the scale in parentheses)**

Method	Luminosity, pb^{-1}	Expected signal	Expected background	Expected σ_{stat}, GeV/c^2
NWA	360	19.4 ± 1.4 (99.8%)	14.1 ± 3.5 (96%)	12.8 (1.060)
KIN	340	12.9 ± 1.1 (75%)	6.4 ± 1.2 (61%)	15.1 (1.033)
PHI	340	17.2 ± 1.4 (100%)	10.5 ± 1.9 (100%)	14.5 (1.055)

Nonunity width of the pull distribution indicates that the statistical uncertainty is underestimated for the analysis. Therefore, the uncertainties obtained from the likelihood fit on the data are scaled by the underestimation determined from the pseudoexperiments. Using the $m_t = 178$ GeV/c^2 HERWIG simulation and assuming a $t\bar{t}$ cross section of 6.1 pb, Table 4 compares the expected statistical uncertainty of the three measurement techniques after applying this correction due to observed pull width (shown in parentheses).

5. SYSTEMATIC UNCERTAINTIES

Apart from the statistical uncertainty on the measured top-quark mass due to the limited size of our data sample, there are several sources of systematic uncertainty. These systematic effects come from uncertainty in the Monte Carlo simulation of $t\bar{t}$ and background events, from mismodeling by the simulation of the detector response to leptons and jets, and from the validity of various assumptions made during the implementation of the mass measurement techniques.

5.1. Systematic Uncertainties for ℓ + Jets Methods. There are a number of additional systematic uncertainties that affect both analyses: initial-state and final-state radiation uncertainties (ISR/FSR), uncertainties arising from the parton distribution functions (PDFs), and uncertainties arising from modeling of the background processes, the choice of event generators and b-jet fragmentation, decays, and color connections (Modeling) [31]. Table 5 summarizes these uncertainties.

Table 5. **The systematic uncertainties for the two ℓ + jets analyses**

Systematic	$\Delta M_{\rm top}$, GeV/c^2	
	DLM	Template
Jet energy scale	3.0	$\sim 2.5^*$
ISR/FSR	0.6	0.7
PDFs	0.5	0.3
Modeling	0.7	0.9
Method	0.5	0.6
Total	3.2	1.3^*

*The JES uncertainty is included in the uncertainty reported by the likelihood fit.

The DLM method has additional uncertainties that arise from the use of transfer functions and from the procedure that corrects the measured mass for the presence of background (Method). Together with the JES and other common sources noted above, the systematic uncertainty on the DLM mass measurement is 3.2 GeV/c^2.

The template method has additional uncertainties arising from the statistical precision of the templates themselves and approximations made in treating JES as a single parameter affecting all jets coherently (Method). The total systematic uncertainty on the template mass measurement is 1.3 GeV/c^2.

5.2. Systematic Uncertainties for Dilepton Methods. As such, most sources of systematic uncertainty are common to all mass analyses, and are estimated by adjusting a particular input value to the simulation and constructing new mass templates. The pseudoexperiments are performed using events drawn from the new mass templates, and comparing the resulting median reconstructed top-quark mass with that of the nominal simulation. The sources of systematic uncertainty within each mass analysis are assumed to be uncorrelated, so that a total systematic uncertainty for each method is calculated as the sum in quadrature of the various sources, as summarized in Table 6.

Table 6. **Summary of the systematic uncertainties on the top-quark mass measurement (in GeV/c^2) for the NWA, KIN, and PHI analyses**

Systematic source	NWA	KIN	PHI
Jet energy scale	3.4	3.2	3.5
b-jet energy	0.6	0.6	0.7
MC generator	0.5	0.6	0.7
PDFs	0.5	0.5	0.6
ISR	0.6	0.6	0.6
FSR	0.5	0.3	0.4
Background shape	2.6	1.6	1.5
Template statistics			
Signal	0.2	0.4	n/a
Background	1.3	1.2	n/a
Total	4.6	4.0	4.0

Note. The total uncertainty is obtained by adding the individual contributions in quadrature. (The uncertainty due to signal and background template statistics for the PHI method is accounted for in the total statistical uncertainty.)

One of the largest sources of systematic uncertainty arises from potential mismodeling of the jet-energy measurement, through uncertainties in the various corrections applied to the measured jet energy [20]. These jet-energy corrections involve the nonuniformity in response of the calorimeter as a function of η, effects from multiple $p\bar{p}$ collisions, the absolute jet-energy scale for hadrons, energy deposition from the underlying $p\bar{p}$ event, and energy loss outside the jet search cone ΔR. A systematic uncertainty is estimated for each jet-energy correction by performing pseudoexperiments drawn from signal and background templates with ± 1 standard deviation in correction uncertainty, and taking the half-difference in median reconstructed top-quark mass between the two results. The uncertainties from each energy correction are then added in quadrature to arrive at a total systematic uncertainty on the jet-energy scale.

Since the above jet-energy corrections are developed from studies of samples dominated by light quark and gluon jets, additional uncertainty occurs from extrapolating this procedure to b quarks [8]. As in the jet-energy scale uncertainty, pseudoexperiments are performed on events where the b-jet energies have been altered by ± 1 standard deviation for uncertainty, and the resulting half-differences used to estimate the systematic uncertainty due to b-jet energy uncertainty.

Several systematic uncertainties are due to the modeling of the $t\bar{t}$ signal.

The effects of the particular Monte Carlo generator chosen by comparing pseudoexperiments drawn from PYTHIA simulation with events taken from our

nominal signal templates constructed using HERWIG are studied. These generators differ in their hadronization models and in their handling of the underlying $p\bar{p}$ event and multiple $p\bar{p}$ interactions [31]. We take the difference in reconstructed top-quark mass between HERWIG and PYTHIA pseudoexperiments as the systematic uncertainty due to choice of generator.

The systematic uncertainty associated with the initial state radiation (ISR) is studied by changing the QCD parameters for parton shower evolution according to comparisons between CDF Drell–Yan data and simulation [8]. Since final-state radiation (FSR) shares the same Monte Carlo shower algorithms as ISR, these variations in QCD parameters are used to generate FSR systematic samples by varying a set of parameters specific to FSR modeling. One then compares the reconstructed top-quark mass from samples with increased and decreased ISR and FSR to estimate the systematic uncertainty due to these sources. The uncertainty in reconstructed top-quark mass from our choice of parton distribution function (PDF) is found by comparing two different groups (CTEQ5L [26] and MRST72 [32]). Additionally, MRST72 and MRST75 sets, derived using different $\Lambda_{\rm QCD}$ values, are compared, and 20 eigenvectors within the CTEQ6M group are varied by ± 1 standard deviation. Differences in pseudoexperiment results from these variations are added in quadrature to arrive at a total systematic uncertainty from the choice of PDF. Further studies comparing LO with NLO $t\bar{t}$ Monte Carlo show a negligible effect on the reconstructed top-quark mass.

Since the background template is also derived from simulation, another source of systematic uncertainty reflects the potential mismodeling by the Monte Carlo of the background shape. This uncertainty is estimated by measuring the effect on top-quark mass from pseudoexperiments where the relative combination of Drell–Yan and fake backgrounds (the largest two sources) is adjusted by predicted uncertainty.

The finite statistics in the simulated signal and background templates result in a systematic uncertainty on the parameterized p.d.f's used in the likelihood (Eq. (29)), even if modeling of the signal and background processes is correct. As described in Sec. 3, the PHI method accounts for this uncertainty in template parameterizations within the statistical uncertainty returned by the likelihood minimization through the term $\mathcal{L}_{\rm param}$ of Eq. (31). The NWA and KIN procedures estimate directly the top-quark mass uncertainty due to finite template statistics, and incorporate this effect into the total systematic uncertainty. For each signal template, we Poisson fluctuate the number of events in each bin to create a new template, which is parameterized according to Eq. (26). We then perform pseudoexperiments drawing signal events from the nominal templates but applying them to a likelihood fit with the fluctuated signal p.d.f. in Eq. (29), producing a distribution of reconstructed top-quark mass. Repeating this procedure many times, we estimate the systematic uncertainty due to limited statistics in the signal templates as the root mean square of the median reconstructed top-quark masses

from the fluctuated pseudoexperiments. In a similar fashion, we estimate the analogous systematic uncertainty due to limited background template statistics by fluctuating each template bin of the various background components.

6. RESULTS

6.1. ℓ + Jets Results. *6.1.1. DLM Method.* There are 63 $t\bar{t}$ candidate events passing the event selection criteria [9]. The joint likelihood of these events is shown in Fig. 13. From the fit, it was obtained $M_{\rm top} = 171.8^{+2.2}_{-2.0}$ (stat. only) GeV/c^2, assuming there is no background. The mapping function was applied to remove the mass-pulling effect of the background. Figure 14 shows the extracted top mass as a function of the background fraction. The top-quark mass changes by $+1.4$ GeV/c^2 for a background fraction of 14.5%.

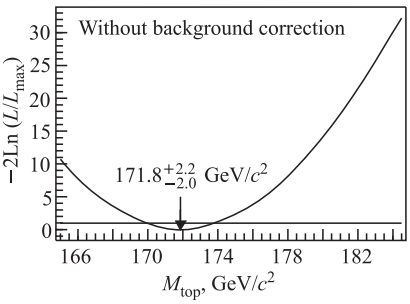

Fig. 13. The joint negative log-likelihood distribution of the 63 events observed in the data. The fit gives $M_{\rm top} = 171.8^{+2.2}_{-2.0}$ GeV/c^2, before any corrections

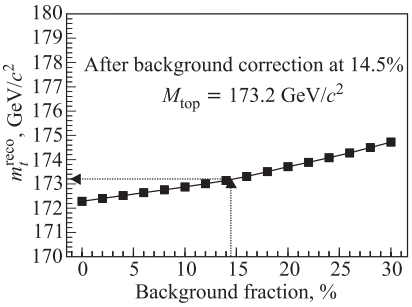

Fig. 14. Extracted top-quark mass using the mapping function as a function of the background fraction

For the final result [9], the estimated 14.5% background fraction was used, which gives $M_{\rm top} = 173.2^{+2.6}_{-2.4}$ (stat. only) GeV/c^2.

6.1.2. Template Method. The four reconstructed top-quark mass distributions and the results of the fit for template method [8] are shown in Fig. 15, where we also show the background contributions. In all cases, one sees agreement between the observed data distributions and the fitted curves. One obtained $M_{\rm top} = 173.5^{+3.7}_{-3.6}$ (stat.) GeV/c^2, where the uncertainty is statistical and incorporates the uncertainty due to JES, which we estimate contributes ~ 2.5 GeV/c^2. Figure 16 shows the likelihood in the $M_{\rm top}-$JES plane. If one does not constrain JES to the nominal value of zero, one obtains JES $= -(0.25 \pm 1.22)\sigma_c$, which indicates that our nominal jet-energy calibrations are in good agreement with information

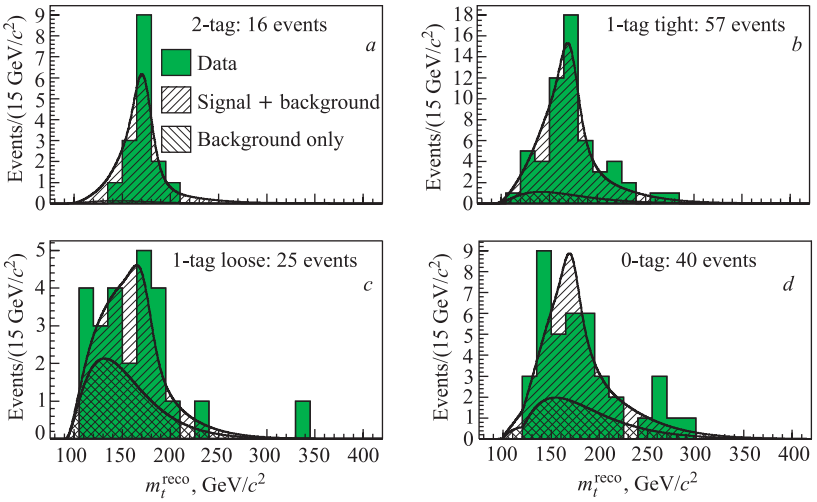

Fig. 15. The m_t^{reco} distribution of the template method is shown for each subsample overlaid with the expected distribution using M_{top}, JES, and signal and background normalizations from the combined fit. The events with $\chi^2 > 9$ have been excluded from each subsample

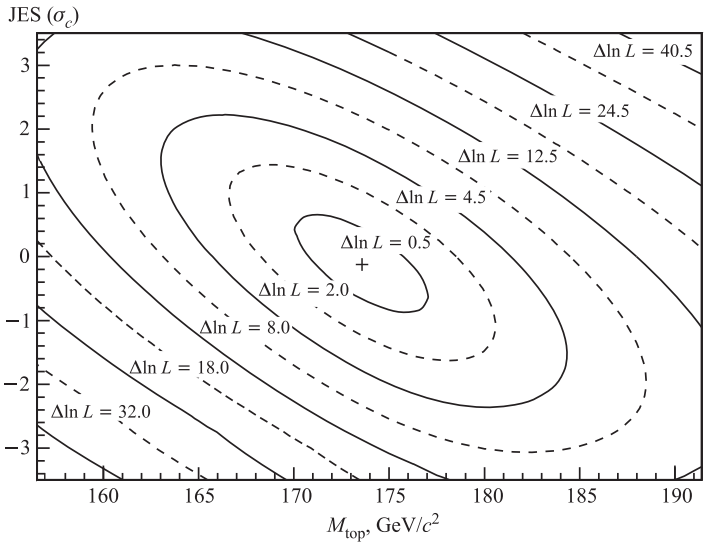

Fig. 16. Contours of the template method likelihood are shown in the $M_{\text{top}}-$JES plane for the combined fit to all four subsamples. The crosshair shows the best fit point. Contours are given at intervals of $\Delta \ln L$, the deviation in log-likelihood from its maximum

provided by the W-boson mass peak in the $t\bar{t}$ decay. This also demonstrates that the JES constraint from the W-boson decay has comparable precision to the jet-energy calibration.

6.2. Dilepton Results. The NWA procedure is applied to the 46 events satisfying the LTRK selection in 360 pb^{-1} of Run-II data, with 45 events resulting in NWA solutions [28]. The KIN and PHI analyses are applied to the 33 events of the DIL selection sample, corresponding to 340 pb^{-1} [28]. Of this sample, 30 events pass kinematic reconstruction in the KIN method, while the PHI analysis returns solutions for all 33 events. Each method applies the likelihood procedure described in Sec. 3, using the expected number of background events listed in Table 4 for the LTRK or DIL selection sample after accounting for mass reconstruction efficiency. As listed in Table 7, each likelihood fit returns a constrained number of background events consistent with the expected value. The number of signal events returned from each likelihood fit ensures that the total number of events in the likelihood agrees with that observed, thereby accounting for the upward fluctuations in both the DIL and LTRK selection samples.

Table 7. **Summary of results for the NWA, KIN, and PHI methods applied to the LTRK and DIL data samples. Listed for each method are: number of total observed events in the sample, number of events with mass solutions, expected number of background events, constrained likelihood fit values for signal and background events and top-quark mass, and unconstrained likelihood mass**

Method	Data sample			Constrained results			Unconstrained
	$N_{\rm tot}$	$N_{\rm sol}$	$n_b^{\rm exp}$	n_s	n_b	m_t, GeV/c^2	m_t, GeV/c^2
NWA	46	45	14.1 ± 3.5	32.4 ± 7.4	13.4 ± 3.5	$170.7^{+6.9}_{-6.5}$	168.3 ± 4.9
KIN	33	30	6.4 ± 1.2	24.5 ± 5.6	6.1 ± 1.7	$169.5^{+7.7}_{-7.2}$	168.4 ± 6.1
PHI	33	33	10.5 ± 1.9	24.4 ± 5.9	10.0 ± 1.9	$169.7^{+8.9}_{-9.0}$	169.2 ± 6.4

Figure 17, *a* shows for the PHI method, the reconstructed top-quark mass in the data, the normalized background and signal+background shapes, and the variation of $-\ln(\mathcal{L}/\mathcal{L}_{\max})$ as a function of the top-quark mass hypothesis. For each method, the final top-quark mass is taken as the value of m_t which minimizes the likelihood function. Statistical uncertainties are obtained by taking the width at $-\ln(\mathcal{L}/\mathcal{L}_{\max}) + 0.5$, and adjusting for the underestimation found in pull widths. Table 7 summarizes the measured top-quark mass and statistical uncertainty for the three mass methods after pull width corrections.

Figure 17, *b* compares the measured statistical uncertainties of the PHI method with pseudoexperiments using the $m_t = 170$ GeV/c^2 sample which has the same number of events as that observed in the data. We find the probabilities for achieving the observed statistical uncertainties to be 9, 23, and 19% for the NWA,

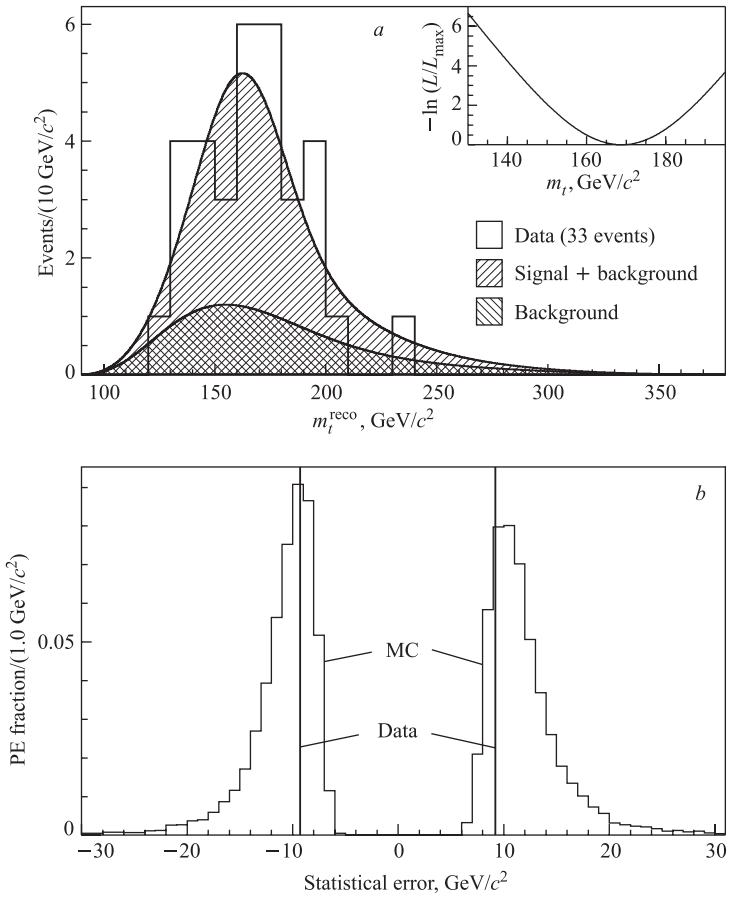

Fig. 17. Results for the PHI method applied to the 33-event DIL data sample. *a*) Reconstructed top-quark mass for the data events (histogram), with normalized background and signal + background p.d.f. curves, and the likelihood function (inset). *b*) Comparison of measured positive and negative statistical uncertainties in the data sample (vertical lines) with pseudoexperiments generated using the 170 GeV/c^2 signal template

KIN, and PHI methods, respectively. As a further cross-check, one removes the Gaussian constraint on the number of background events in the likelihood procedure (i.e., the term $\mathcal{L}_{n_b}$ in Eq. (28)). For all three methods, this unconstrained fit converges near zero background events, and the resulting top-quark mass, corrected for pull width, is consistent with the constrained result (as seen in Table 7).

7. SUMMARY

Two methods of the top-quark mass measurement in lepton + jets mode are reviewed. The analysis using the Dynamical Likelihood Method [9] results in $M_{\rm top} = (173.2^{+2.6}_{-2.4}\ (\text{stat.}) \pm 3.2\ (\text{syst.}))\ \text{GeV}/c^2$; the analysis using the template technique [8] results in $M_{\rm top} = (173.5^{+3.7}_{-3.6}\ (\text{stat.}) \pm 1.3\ (\text{syst.}))\ \text{GeV}/c^2$. There is a large statistical correlation between these measurements due to the common data sample, so that CDF quotes as a result only the more accurate measurement (obtained with Dubna group participation), the template method result of $M_{\rm top} =$

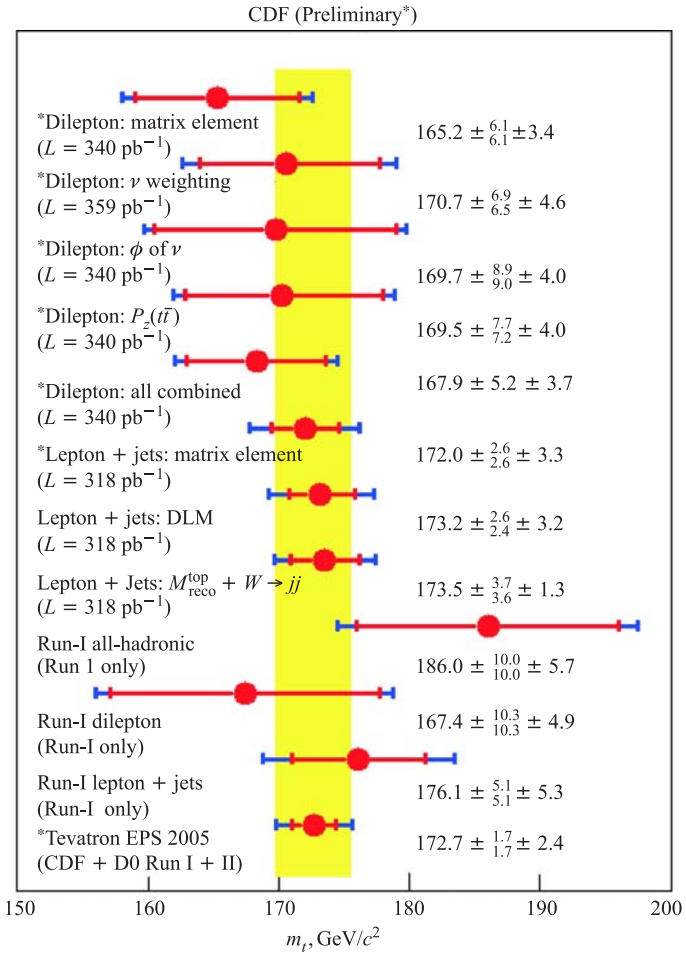

Fig. 18. The summary of the CDF top-mass measurements at the end of 2005

$173.5^{+3.9}_{-3.8}$ GeV/c^2. This provides the most precise currently available single measurement on this important physical parameter.

For dilepton mode we describe three methods [28]. One method, the Neutrino Weighting Algorithm, measures a top-quark mass of $(170.7^{+6.9}_{-6.5}\ (\text{stat.}) \pm 4.6\ (\text{syst.}))$ GeV/c^2. The second technique, called the Full Kinematic Analysis, results in a mass measurement of $(169.5^{+7.7}_{-7.2}\ (\text{stat.}) \pm 4.0\ (\text{syst.}))$ GeV/c^2. The third analysis using the Neutrino ϕ Weighting Method measures a value of $(169.7^{+8.9}_{-9.0}\ (\text{stat.}) \pm 4.0\ (\text{syst.}))$ GeV/c^2. Accounting to correlations in the statistical and systematic uncertainties between the methods, CDF combines three results, giving a top-quark mass in the dilepton channel of $(170.1 \pm 6.0\ (\text{stat.}) \pm 4.1\ (\text{syst.}))$ GeV/c^2.

We reviewed here one template method and one Matrix Element Technique method for lepton + jets top decay mode as well as three different template methods for dilepton top decays. Finally, the CDF top-mass measurements table at the end of 2005 is presented in Fig. 18.

REFERENCES

1. *Abe F. et al. (CDF Collab.)* // Phys. Rev. Lett. 1995. V. 74. P. 2626;
   Abachi S. et al. (DØ Collab.) // Ibid. P. 2632.
2. *CDF and (DØ Collab.) and the Tevatron Electroweak Working Group.* hep-ex/0404010.
3. *Hashimoto M., Tanabashi M., Yamawaki K.* Top Mode Standard Model with Extra Dimensions // Phys. Rev. D. 2001. V. 64. P. 056003;
   Miransky V. A., Tanabashi M., Yamawaki K. Is the T Quark Responsible for the Mass of W and Z Bosons? // Mod. Phys. Lett. A. 1989. V. 4. P. 1043.
4. *Altarelli G., Grunewald M. W.* Precision Electroweak Tests of the Standard Model // Phys. Rep. 2004. V. 403–404. P. 189–201;
   Xiao Z. J. et al. Implications of the Top-Quark Mass Measurement for the SM Higgs Boson Mass $M(H)$ // J. Phys. G. 1995. V. 21. P. 19.
5. *Bellettini G. et al. (CDF Collab.).* Measurement of the Top-Quark Mass Using the MINUIT Fitter in Dilepton Events at CDF. FERMILAB-pub-05-564-e-td; JINR, E1-2005-18. Dubna, 2005. 12 p.
6. *Bellettini G. et al. (CDF Collab.).* Top-Quark Mass Measurement in Non-Tagged Lepton + Jets Events at CDF. FERMILAB-pub-05-565-e; JINR, E1-2005-17. Dubna, 2005. 8 p.
7. *Bellettini G. et al. (CDF Collab.).* Measurement of the Top-Quark Mass Using Neuitrino Phi Weighting Method in Dilepton Events at CDF. CDF/anal/top/public/7759; JINR, E1-2005-129. Dubna, 2005. 12 p.
8. *Acosta D. et al. (CDF Collab.).* Top-Quark Mass Measurements Using the Template Method in the Lepton + Jets Channel at CDF II // Phys. Rev. D. 2006. V. 73. P. 032003.
9. *Abulencia A. et al. (CDF Collab.).* Measurement of the Top Quark Mass with the Dynamical Likelihood Method Using Lepton Plus Jets Events with b Tags in p anti $-p$ Collisions at $\sqrt{s} = 1.96$ TeV // Phys. Rev. D. 2006. V. 73. P. 092002.
10. *Acosta D. et al.* // Phys. Rev. D. 2005. V. 71. P. 032001;
    The CDF II Detector Technical Design Report. Fermilab-Pub-96/390-E.

11. *Hill C. S.* // Nucl. Instr. Meth. A. 2004. V. 530. P. 1;
Sill A. et al. // Nucl. Instr. Meth. A. 2000. V. 447. P. 1;
Affolder A. et al. // Ibid. V. 453. P. 84.

12. *Affolder T. et al.* // Nucl. Instr. Meth. A. 2004. V. 526. P. 249.

13. *Albrow M. et al.* // Nucl. Instr. Meth. A. 2002. V. 480. P. 524–545;
Apollinari G. et al. // Nucl. Instr. Meth. A. 1998. V. 412. P. 515–526.

14. *Balka L. et al.* // Nucl. Instr. Meth. A. 1988. V. 267. P. 272–279;
Hahn S. R. et al. // Ibid. P. 351–366;
Bertolucci S. et al. // P. 301–314.

15. *Ascoli G. et al.* // Nucl. Instr. Meth. A. 1988. V. 268. P. 33;
Dorigo T. et al. // Nucl. Instr. Meth. A. 2001. V. 461. P. 560.

16. *D. Acosta et al.* // Nucl. Instr. Meth. A. 2002. V. 494. P. 57.

17. *Acosta D. et al. (CDF Collab.)* // Phys. Rev. D. 2005. V. 71. P. 052003.

18. *Acosta D. et al. (CDF Collab.)* // Phys. Rev. Lett. 2004. V. 93. P. 142001-1.

19. *Abe F. et al. (CDF Collab.)* // Phys. Rev. Lett. 1998. V. 80. P. 2779.

20. *Bhatti A. et al.* // Nucl. Instr. Meth. A (in press).

21. *Sjostrand T. et al.* // Comp. Phys. Commun. 2001. V. 135. P. 238.

22. *Cacciari M. et al.* // J. High Energy Phys. 2004. V. 404. P. 068.

23. *Mangano M. L. et al.* // J. High Energy Phys. 2003. V. 307. P. 001.

24. *Corcella G. et al. (HERWIG 6).* An Event Generator for Hadron Emission Reactions with Interfering Gluons (Including Supersymmetric Processes) // JHEP. 2001. 01. 10.

25. *Eidelman S. et al. (Particle Data Group)* // Phys. Lett. B. 2004. V. 592. P. 1.

26. *Lai H. L. et al.* // Eur. Phys. J. C. 2000. V. 12. P. 375.

27. *Abe F. et al. (CDF Collab.)* // Phys. Rev. Lett. 1999. V. 82. P. 271;
Affolder T. et al. (CDF Collab.) // Phys. Rev. D. 2001. V. 63. P. 032003.

28. *Abulencia A. et al. (CDF Collab.).* Measurement of Top-Quark Mass Using Template Methods on Dilepton Events in $p\bar{p}$ Collisions at $\sqrt{s} = 1.96$ TeV // Phys. Rev. D. 2006. V. 73. P. 112006.

29. *Abbott B. et al. (DØ Collab.)* // Phys. Rev. D. 1999. V. 60. P. 052001.

30. *Press W. et al.* Numerical Recipes in C: The Art of Scientific Computing. Cambridge Univ. Press, 1992.

31. *Sjostrand T.* // Comp. Phys. Commun. 1994. V. 82. P. 74;
Marchesini G. et al. // Comp. Phys. Commun. 1991. V. 67. P. 465.

32. *Martin A. D. et al.* Implementation from PDFLIB: The Parton Density Functions Library, Version 8.04, MRST set 75, CERN // Eur. Phys. J. C. 1998. V. 4. P. 463.